Title: Xenotropic and polytropic retrovirus receptor 1 regulates procoagulant platelet polyphosphate

Short title: XPR1 regulates polyP

Author list: Reiner K. Mailer[1,¶], Mikel Allende[1,2,¶], Marco Heestermans[1], Michaela Schweizer[3], Carsten Deppermann[1], Maike Frye[1], Giordano Pula[1], Jacob Odeberg[4], Mathias Gelderblom[5], Stefan Rose-John[6], Albert Sickmann[7], Stefan Blankenberg[8], Tobias Huber[9], Christian Kubisch[10], Coen Maas[11], Stepan Gambaryan[12], Dmitri Firsov[13], Evi X. Stavrou[14,15], Lynn Butler[1,4], Thomas Renné[1*]

¶ These two authors contributed equally to this work

Affiliations:
[1] Institute of Clinical Chemistry and Laboratory Medicine, University Medical Center Hamburg-Eppendorf, Hamburg, Germany
[2] Department of Molecular Medicine and Surgery, Karolinska Institute, Stockholm, Sweden
[3] Electron Microscopy Unit, Center for Molecular Neurobiology (ZMNH), University Medical Center Hamburg-Eppendorf, Hamburg, Germany
[4] K.G. Jebsen Thrombosis Research and Expertise Centre (TREC), Department of Clinical Medicine, The Arctic University of Norway, Tromsø, Norway
[5] Department of Neurology, University Medical Center Hamburg-Eppendorf, Hamburg, Germany
[6] Institute of Biochemistry, University of Kiel, Kiel, Germany
[7] Leibniz-Institut für Analytische Wissenschaften - ISAS - e.V., Dortmund, Germany
[8] Department of General and Interventional Cardiology, University Heart Center, Hamburg, Germany
[9] III. Department of Medicine, University Medical Center Hamburg-Eppendorf, Hamburg, Germany
[10] Institute of Human Genetics, University Medical Center Hamburg-Eppendorf, Hamburg, Germany
[11] Department of Clinical Chemistry and Haematology, University Medical Center Utrecht, Utrecht, University, Utrecht, the Netherlands
[12] Sechenov Institute of Evolutionary Physiology and Biochemistry, Russian Academy of Sciences St. Petersburg, Russia
[13] Department of Pharmacology and Toxicology, University of Lausanne, Lausanne, Switzerland
[14] Department of Medicine, Louis Stokes Cleveland VA Medical Center, Cleveland, Ohio, United States
[15] Department of Medicine, Case Western Reserve University School of Medicine, Cleveland, Ohio, United States

* Corresponding author
Thomas Renné, M.D. Ph.D.
University Medical Center Hamburg-Eppendorf
Institute of Clinical Chemistry and Laboratory Medicine (O26), Martinistrasse 52
D-20246 Hamburg, Germany
Tel: +49-40-7410 58984
Fax: +49-40-7410 57576
Email: thomas@renne.net

Abstract word count: 159

Text word count: 4764

Figure Count: 6

Supplemental Figure count: 7

Table Count: 1

Supplemental Table count: 0

Reference count: 69

Key points

1) Xenotropic and polytropic retrovirus receptor 1 (XPR1) is a major phosphate exporter in platelets.

2) Inhibiting XPR1 in platelets increases procoagulant polyphosphate levels and augments arterial and venous thrombosis without affecting hemostasis in mice.

ABSTRACT

Polyphosphate is a procoagulant inorganic polymer of linear linked orthophosphate residues. Multiple investigations have established the importance of platelet polyphosphate in blood coagulation, however the mechanistic details of polyphosphate homeostasis in mammalian species remain largely undefined. Here, we show that xenotropic and polytropic retrovirus receptor 1 (XPR1) regulates polyphosphate in platelets and is implicated in thrombosis *in vivo*.

We used bioinformatic analyses of omics data to identify XPR1 as a major phosphate transporter in platelets. *Xpr1* mRNA and protein expression inversely correlated with intracellular polyphosphate content and release. Pharmacological interference with XPR1 activity increased polyphosphate stores, led to enhanced platelet-driven coagulation and amplified thrombus formation under flow via the polyphosphate/factor XII pathway. Conditional gene deletion of *Xpr1* in platelets resulted in polyphosphate accumulation, accelerated arterial thrombosis, and augmented activated platelet-driven pulmonary embolism without increasing bleeding in mice.

These data identify platelet XPR1 as an integral regulator of platelet polyphosphate metabolism highlighting a fundamental role for phosphate homeostasis in thrombosis.

INTRODUCTION

Inorganic polyphosphate (polyP) is a linear polymer of tens to hundreds of phosphate residues linked via high-energy phosphoanhydride bonds. This evolutionary ancient polyanion is ubiquitously found in nature including bacterial, fungal, plant, animal and human cells [1]. Despite its structural simplicity, polyP exerts a number of distinct, intracellular activities. The polymer contributes to energy homeostasis and functions as a storage pool for inorganic phosphate (P_i) [2-4].

Regulation of polyP has remained poorly understood in metazoans but has been characterized in detail, in prokaryotes and yeast. *Saccharomyces cerevisiae* express four distinct P_i transporters (Pho84, Pho87, Pho90, and Pho89) [5] that mediate uptake of extracellular P_i into the cytosol; deficiency in individual P_i transporters reduces polyP formation [6]. Genetic analyses in yeast confirmed a correlation between intracellular P_i levels and polyP content; strains with low imported P_i also exhibited reduced intracellular polyP [7] and *vice versa*, polyP levels are reduced when budding *Saccharomyces cerevisiae* are switched from P_i-rich to P_i-starvation media [8,9]. Some bacteria such as *Acinetobacter johnsonii* and the parasite *Trypanosoma cruzi* (the etiologic agent of Chagas disease) accumulate up to 30% of their dry cell weight as intracellular granules referred to as acidocalcisomes, which are calcium- and polyP-rich organelles [10,11]. In some mammalian cells, polyP is stored in organelles that function similar to acidocalcisomes including mast cell and basophil granules [12], astrocyte vesicles [13] and platelet dense granules [14] that allow for rapid release of preformed polyP into the interstitial and vascular spaces. However, only small amounts of soluble short-chain polymers are found in the supernatant of activated platelets, whereas the majority is retained on the plasma membrane as insoluble, calcium-rich nanoparticles [15,16]. Platelet polyP has been recognized as a procoagulant mediator with a multitude of functions in the coagulation system that include activation of factor XII (FXII), which in turn triggers the "intrinsic" pathway of coagulation [15,17-21]. The sum of polyP-mediated procoagulant activities leads to enhanced clotting in human plasma and increased thrombosis in animal models [22,23].

Xenotropic and polytropic retrovirus receptor 1 (XPR1) is an eight-pass transmembrane molecule of 696 amino acids that was initially recognized as a cell-surface receptor for xenotropic and polytropic murine leukemia retroviruses (X- and P-MLV) [24]. Recent work in mammalian cells revealed that XPR1 is involved in P_i export and leads to depletion of intracellular P_i [25,26]. In yeast and excavate eukaryotes, XPR1 expression has been linked to polyP metabolism. *Trypanosoma cruzii* expresses a

4

XPR1 homologous protein TcPho91, and modulation of TcPho91 activity influences intracellular polyP levels [27]. Consistently, deficiency in the XPR1 homolog Pho91 in yeast increases intracellular P_i and polyP levels [6].

Despite its fundamental functions, polyP regulation in mammalian cells has remained largely undefined. Here, we tested the hypothesis that polyP levels are regulated in response to P_i homeostasis. Using omics data resources, we identified XPR1 as a major P_i transporter in platelets. We determined that pharmacologic and genetic interference with XPR1 led to intracellular polyP accumulation. Similarly, targeting XPR1 in platelets increased polyP content, augmented activated platelet-driven coagulation and led to thrombus formation under flow in a FXII-dependent manner. Conditional ablation of *Xpr1* in platelets accelerated vascular occlusion in murine models of venous and arterial thrombosis without affecting hemostasis. Taken together, the present study provides experimental evidence that XPR1 is a key regulator of platelet polyP and reveals an unidentified role of P_i homeostasis in thromboembolic disease.

METHODS

Detailed description of antibodies, reagents, and additional methods can be found in the Supplemental Methods section (available on the *Blood* website).

Platelet Xpr1-deficient mouse strains

Xpr1^{fl/fl} mice carrying *loxP* sites on either side of *Xpr1* exon 2 were previously described [28]. *Xpr1*^{fl/fl} mice were bred with *Pf4-Cre* transgenic animals to delete *Xpr1* specifically in the megakaryocyte/platelet lineage. All mice were treated according to national guidelines for animal care at the animal facilities of University Medical Center Hamburg-Eppendorf and approved by local authorities (#76/16). For animal experiments, 8 to 14-week old mice of either sex (1:1 ratio) were utilized. All procedures were conducted in accordance with 3Rs regulations.

PolyP extraction and quantification

PolyP was isolated from HEK293 or MEG-01 cells using anion exchange columns [29]. Briefly, cells were incubated with sodium chloride (4 M) for 5 min, diluted with 50 mM Tris, pH 8.1, incubated with DNase I (200 U ml^{-1}) and proteinase K (750 µg ml^{-1}; Sigma-Aldrich) for 1 h at 37°C, and centrifuged at 14,000 *g* for 8 min to remove debris. Lysates were diluted in buffer QG (Qiagen) and applied to QIAquick Spin Columns (Qiagen). Columns were washed twice with washing buffer and polyP was eluted in 50 mM Tris buffer. Isolated material was subjected to 1 h incubation with 10 µg ml^{-1} recombinant *E. coli* exopolyphosphatase (PPX) at 37°C that ablated purified polyP procoagulant activity [30]. Released orthophosphate was estimated using a phosphate assay kit (Abcam; Cambridge, UK), according to manufacturer's instructions. P$_i$ concentrations attributed to polyP were quantified by calculating the difference of PPX-treated and untreated samples.

Soluble and membrane-associated insoluble polyP measurements

Washed human platelets were incubated with XVDL and/or PVDL for up to 24 h prior to polyP measurements. Flow cytometry analyses probing for surface expression of P-selectin (CD62P) (clone: Psel.KO.2.7, Bio-Rad; 1:100 dilution) indicated that platelets were not activated during the incubation period. Quantification of soluble and membrane-associated insoluble polyP was performed as previously described [16]. Briefly, washed human or *Xpr1*^{fl/fl}, *Xpr1*^{fl/+} *Pf4-Cre* and *Xpr1*^{fl/fl} *Pf4-Cre* mouse platelets were incubated for 20 min with Horm collagen (10 µg ml^{-1}) in HEPES-Tyrode´s buffer. Supernatants containing soluble polyP were incubated for 2 h with buffer or PPX (50

µg ml^{-1}) at 37°C and P$_i$ concentrations were determined by the malachite green-based phosphate assay kit (Abcam) [30]. To measure insoluble membrane-associated polyP, collagen-stimulated platelets were incubated with 250 mM EDTA for 15 min at 37°C to dissociate membrane-retained Ca^{2+}-polyP nanoparticles [16] followed by PPX digestion, as above.

RESULTS

XPR1 is a major phosphate transporter in platelets

Ten distinct phosphate transporters including XPR1, SLC17A1-4, SLC20A1-2 (P_iT-1 and P_iT-2) and SLC34A1-3 have been described in eukaryotic systems [25,31]. To predict P_i transporter expression in platelets, we sourced RNAseq data of unfractionated human bone marrow, generated as part of the Human Protein Atlas project (https://www.proteinatlas.org/). XPR1, SLC20A1 and SLC20A2 were the only P_i transporters with detectable mRNA expression in the bone marrow (**Figure 1A**). To confirm transporter expression in circulating cells in an independent dataset, RNAseq data from unfractionated human whole blood samples (n = 407) was downloaded from GTEx Analysis V7 (https://gtexportal.org/home/). In all samples, *XPR1*, *SLC20A1* and *SLC20A2* mRNA was detected (mean fragments per kilobase of exon model per million reads mapped [FPKM] 2.6, 25.7 and 1.74, respectively). We next examined which of these transporters were expressed in platelets using the platelet web database (http://plateletweb.bioapps.biozentrum.uni-wuerzburg.de/plateletweb.php) [32]. XPR1 expression was detected in human platelets both on mRNA [33] and protein level [34] but SLC20A1 and SLC20A2 were not. To validate our findings, we probed for XPR1 protein in membrane fractions of human and murine platelets. Antibodies against the N- and C-terminus of XPR1 detected a single band in human (**Figure 1B**) and mouse (**Figure 1C**) platelet membrane fractions, migrating at an apparent molecular weight of ~65 kDa (**Supplemental Figures 1A - 1D**). Recombinant human XPR1 expressed in HEK293 cells migrated with a similar apparent molecular weight and served as control. Consistent with cell surface localization of XPR1 in adherent cells [26], immunofluorescence microscopy visualized XPR1 at the plasma membrane in non-permeabilized human platelets (**Figure 1D**). To assess the subcellular localization of platelet XPR1 on an ultra-structural level, platelets were analyzed by transmission electron microscopy. Immunogold labelling showed that XPR1 was enriched at the plasma membrane (**Figure 1E**). These data indicated that XPR1 is a major phosphate transporter in platelets.

XPR1 expression inversely correlates with polyP levels

In infra-mammalian systems, XPR1 homologous proteins TcPho91 and Pho91 regulate polyP levels [6,27]. We hypothesized that XPR1 similarly controls polyP in platelets and examined if there is a correlation between XPR1 expression and intracellular polyP levels. Transient overexpression of XPR1 in HEK293 cells (**Figure 2A**) and MEG-01 megakaryocytes (**Figure 2B**) increased XPR1 signal intensity in

western blots by 8- and 45-fold compared to mock control, respectively. The increased XPR1 expression dose-dependently reduced total polyP content to 65 ± 3% and 58 ± 9%, respectively compared to levels in mock vector-transfected HEK293 (**Figure 2C**) and MEG-01 (**Figure 2D**) cells (set to 100% each). *Vice versa,* interference with XPR1 expression using siRNA-mediated knock-down decreased *XPR1* mRNA leading to increased polyP levels in HEK293 (up to 138 ± 3%; **Figure 2E**) and MEG-01 cells (up to 129 ± 5%; **Figure 2F**). siRNA treatment did not affect cell morphology or levels of the housekeeping vasodilator-stimulated phosphoprotein (VASP, not shown). Chain length of polyP molecules ranged between 50 - 400 and 40 - 200 P_i moieties in control-treated HEK293 and MEG-01 cells, respectively (**Figures 2G, 2H**). XPR1 overexpression in these cell types only slightly reduced polyP size (**Figure 2G**; 50 - 150 and 40 - 140 mers). Accordingly, *XPR1* knockdown had only minor impact on average polyP size or degree of dispersion in HEK293 and MEG-01 cells on day 3 (**Figure 2H**). We used exopolyphosphatase (PPX), an enzyme that specifically degrades polyP [30,35] and confirmed that the cell-purified material was indeed, polyP. Together, these data show that polyP content is inversely proportional to XPR1 expression levels.

Inhibition of platelet XPR1 increases intracellular polyP content

XPR1 is the entry receptor for X-MLV [36,37] and an XPR1 ligand derived from the X-MLV envelope-receptor-binding domain (XVDL), inhibits XPR1-mediated P_i export leading to increased P_i in adherent cells [26]. To pharmacologically target XPR1 activity, we cloned and expressed in *E. coli* XVDL and the corresponding P-MLV envelope ligand (PVDL, negative control; schematically shown in **Supplemental Figures 2A**, **2B**). While X-MLV and P-MLV differ in their activities, they share high sequence homology with each other [38, 26]. Coomassie brilliant blue-stained PAGE and immunoblot analyses confirmed the purity of recombinant XVDL and PVDL ligands (**Supplemental Figures 2C**, **2D**).

Washed human platelets were incubated with increasing concentrations (2 - 200 µg ml^{-1}) of XVDL or PVDL for up to 24 h. Virus-derived ligands did not activate platelets (data not shown). PolyP was subsequently isolated from treated cells at various time points by anion exchange chromatography and quantified as monophosphate units following PPX digestion with malachite green-based colorimetric assay [30]. Dose-dependently, XVDL treatment significantly increased platelet polyP content (up to 134 ± 7% polymer level) compared to buffer-incubated controls (set at 100%; **Figure 3A**). PolyP levels increased after 4 h of incubation with XVDL and remained elevated for 24

h. PVDL was inactive in altering platelet polyP (**Figure 3B**). X- and P-MLV compete with each other for binding to XPR1 [39]. We tested PVDL for its interference with XVDL-mediated increase of polyP. PVDL competed with XVDL-induced increase in platelet polyP in a dose-dependent manner. PVDL levels as high as 600 µg ml^{-1} completely abolished the effects of XVDL (200 µg ml^{-1}) and restored polyP content to baseline levels (**Figure 3C**). Platelets contain soluble short chain polyP that upon cell activation is released into the supernatant, as well as long(er) chain polyP that is insoluble and retained on the plasma membrane of procoagulant platelets as calcium-rich nanoparticles [16,21]. Here, we examined the impact of targeting XPR1 on each of these distinct polyP pools. Platelets were pre-incubated for 4 h (sufficient for inducing maximum polyP increase) in solution with XVDL, PVDL or buffer prior to activation with Horm collagen. Collagen treatment activates platelets and potently leads to polyP release [16,30,40]. Pre-treating platelets with XVDL, dose-dependently increased soluble polyP in the cell supernatant by 3-fold over polyP levels isolated in supernatant from buffer-treated platelets (1.8 ± 0.2 *vs.* 0.6 ± 0.1 nmol P$_i$ /10^8 platelets, **Figure 3D**); PVDL pre-treatment did not influence soluble polyP levels (**Figure 3E**). Divalent cations mediate the formation and membrane association of insoluble polyP nanoparticles. EDTA (a chelator of divalent ions) disrupts polyP nanoparticles and allows for specific analysis of membrane-associated polyP [16]. Pre-incubation of platelets with XVDL dose-dependently increased membrane-associated insoluble polyP by >2-fold (6.3 ± 0.4 *vs.* 2.6 ± 0.1 nmol/10^8 platelets) compared to buffer pre-treated platelets (**Figure 3F**). In contrast, even at maximum PVDL concentrations, no effect was noted in the amount of cell surface-exposed polyP (**Figure 3G**).

Inhibition of XPR1 amplifies platelet-triggered coagulation via the polyP/FXII-pathway

We next examined if XPR1 increases platelet reactivity in human platelet rich plasma (PRP) using real-time thrombin generation assays (**Figures 3H - 3K**). Consistent with previous data [41,42], collagen-stimulated platelets initiated thrombin formation (**Figures 3H**, **3I**). Pre-incubation with XVDL (**Figure 3H**) but not PVDL (**Figure 3I**), dose-dependently increased collagen-induced platelet procoagulant activity as seen by an increase in total and maximum (peak) thrombin generation by 56% and 143%, respectively compared to buffer pre-incubation of activated platelets (875 ± 95 to 1361 ± 49 nM*min and 47 ± 11 to 114 ± 6 nM at 200 µg ml^{-1} XVDL; **Figures 3J, 3K**). Consistently, targeting XPR1 also shortened the lag time (11.3 ± 1.0 *vs.* 9.1 ± 0.8 min) and time to peak (20.3 ± 1.3 *vs.* 14.7 ± 1.1 min) thrombin formation compared to buffer

control (**Supplemental Figure 3**). To confirm that an increase in platelet polyP rather than other XPR1-mediated events underlies the increase in platelet procoagulant activity, we targeted released polyP in XVDL pre-treated platelets using two strategies: i) recombinant *E. coli* exopolyphosphatase (PPX) which specifically degrades polyP but not other naturally occurring polymers [30], and ii) an enzymatically inactive PPX mutant lacking domains 1 and 2 (PPX_Δ12) that interferes with polyP procoagulant activities without degrading it [30]. Both PPX and PPX_Δ12 reduced thrombin generation induced by synthetic and platelet-derived polyP but did not interfere with tissue factor- or nucleic acid-driven thrombin formation [30]. Addition of PPX and PPX_Δ12 (500 µg ml^{-1} each) to XPR1-inhibited platelets abolished platelet hyperreactivity and thrombin formation triggered by collagen activation was similar to that of unstimulated controls (total: 319 ± 71 and 239 ± 6 *vs.* 299 ± 31 nM*min. Peak thrombin: 15 ± 4 and 11 ± 1 *vs.* 15 ± 1 nM). PolyP initiates coagulation in plasma via contact activation of FXII [15,43]. 3F7 (650 nM) [44], a neutralizing antibody to activated FXII (FXIIa) and rHA-Infestin-4 (500 µg ml^{-1}) [45], a recombinant FXIIa-inhibitor, both blocked the increased procoagulant activity of XVDL/collagen-stimulated platelets. Neutralizing FXIIa and targeting polyP similarly interfered with excess thrombin generation in XVDL/collagen-treated cells (total 527 ± 5 and 547 ± 197 nM*min; peak thrombin 22 ± 1 and 25 ± 9 nM; **Figures 3J**, **3K**). Combination of 3F7 and PPX did not result in further reduction of procoagulant platelet activity (total 522 ± 129 nM*min; peak thrombin 23 ± 7 nM). Together, the data show that XVDL-treated activated platelets trigger excess coagulation by increased polyP/FXII activity in plasma.

Inhibition of XPR1 increases platelet polyP and thrombus formation under flow

At sites of vascular injury, collagen is exposed from the subendothelial matrix resulting in platelet activation and subsequent thrombus formation in a FXII-dependent manner [46]. Therefore, we next investigated if interference with XPR1 augments thrombus formation on collagen-coated surfaces under flow (**Figure 4**). Citrate-anticoagulated human whole blood pre-incubated with increasing doses of XVDL (2 – 200 µg ml^{-1}), was recalcified before being perfused at arterial (**Figure 4A)** and venous (**Figure 4B**) shear rates (1,000 and 100 s^{-1}, respectively). Consistent with earlier data [44,46], in the absence of XVDL platelets adhered to collagen fibers, aggregated, and thrombus formation was observed within 4 min from the time of perfusion (16.5 ± 1.9 and 9.3 ± 0.8% surface coverage by thrombus at arterial and venous shear, respectively). Pre-incubation with XVDL dose-dependently increased thrombus formation by more than 50% compared to untreated control (26.4 ± 2.5 and 17.0 ± 2.5%, respectively). *Vice*

versa, targeting polyP with PPX almost completely abolished thrombosis both at arterial (<5%) and venous (<2%) shear rates. Immunofluorescence microscopy of formed thrombi confirmed the polyP-mediated procoagulant activities of XVDL. Fibrin deposition assessed by fibrin specific antibody 59D8 [47], and platelet accumulation were increased in thrombi following XPR1 inhibition (**Figures 4C**, **4D**). To confirm that XVDL treatment led to increased polyP in platelets, we used fluorescently labeled PPX_Δ12 as a polyP-specific probe [48]. FITC-PPX_Δ12 signal intensity was >70% higher in thrombi produced by XPR1-inhibited platelets over buffer control (10.8 ± 0.2 *vs.* 18.5 ± 1.0 RU at 1,000 s^{-1} and 7.0 ± 0.3 *vs.* 12.2 ± 0.7 RU at 100 s^{-1}; **Figures 4E**, **4F**).

XPR1 deficient platelets have increased polyP content

To characterize the functions of XPR1 in platelets, we targeted its expression selectively in the megakaryocytic/platelet lineage by breeding *Xpr1$^{fl/fl}$* to *Pf4-Cre* transgenic mice. As littermate controls for homozygous conditional *Xpr1* deficiency (*Xpr1$^{fl/fl}$ Pf4-Cre*), we used *Xpr1$^{fl/fl}$* animals lacking *Cre* expression. Additionally, we produced heterozygous *Xpr1$^{fl/+}$ Pf4-Cre* mice having only a single *Xpr1* allele in platelets. PCR confirmed each genotype (**Figure 5A**). *Xpr1* expression in megakaryocytes prepared from a primary bone marrow cell culture of *Xpr1$^{fl/fl}$ Pf4-Cre* mice, was reduced to 45.7 ± 7.9% of levels seen in *Xpr1$^{fl/fl}$* mice (**Figure 5B**). Furthermore, flow cytometry and western blotting confirmed XPR1 protein reduction to 38.2 ± 7.8% and 55.2 ± 7.9%, respectively, in *Xpr1$^{fl/fl}$ Pf4-Cre* megakaryocyte preparations (**Figure 5C**). In line with these data, *Xpr1* expression was virtually absent in *Xpr1$^{fl/fl}$ Pf4-Cre* mouse platelets (7.4 ± 1.8% of *Xpr1$^{fl/fl}$* platelets, **Figure 5D**). XPR1 protein level in platelets from *Xpr1$^{fl/fl}$ Pf4-Cre* mice was reduced to 12.0 ± 5.1% as compared to *Xpr1$^{fl/fl}$* controls (**Figure 5E**) and flow cytometry analyses confirmed loss of XPR1 in *Xpr1$^{fl/fl}$ Pf4-Cre* mouse platelets (**Supplemental Figure 4**). We next asked if reduced platelet XPR1 alone can affect polyP content. In platelets from *Xpr1$^{fl/fl}$ Pf4-Cre* mice, total polyP level was increased by more than 75% over controls (2.60 ± 0.57 *vs.* 1.42 ± 0.34 nmol/10^8 platelets), while a single *Xpr1* allele in *Xpr1$^{fl/+}$ Pf4-Cre* mice was sufficient to maintain polyP close to baseline levels (1.41 ± 0.48 nmol/10^8 platelets; **Figure 5F**). PolyP-specific negative DAPI staining confirmed increased polyP content in isolated platelets of *Xpr1$^{fl/fl}$ Pf4-Cre* mice (not shown). Collagen-activated platelets from *Xpr1$^{fl/fl}$ Pf4-Cre* mice released slightly more soluble polyP into the supernatant as compared to platelets from mice with intact or heterozygous *Xpr1* expression (0.77 ± 0.07 *vs.* 0.66 ± 0.02 and 0.66 ± 0.03 nmol polyP/10^8 platelets; **Figure 5G**), albeit

differences did not reach significance. Quantification of membrane-associated nanoparticle polyP showed that activated platelets of *Xpr1^{fl/fl} Pf4-Cre* mice, expose about 70% more polyP on their cell surface compared to animals with heterozygous or normal *XPR1* expression (1.91 ± 0.09 *vs.* 1.12 ± 0.10 or 1.09 ± 0.10 nmol polyP/10^8 platelets; **Figure 5H**). Hematologic analysis of peripheral blood from *Xpr1^{fl/fl} Pf4-Cre, Xpr1^{fl/+} Pf4-Cre* and *Xpr1^{fl/fl}* mice did not reveal significant differences in platelet counts, platelet morphology (size and volume), production and life span assessed by platelet distribution width or percentage of platelets among other circulating cells (plateletcrit). Similarly, the number of total leukocytes, leukocyte sub-populations as well as red blood cell number and morphology did not differ among *Xpr1^{fl/fl} Pf4-Cre, Xpr1^{fl/+} Pf4-Cre* and *Xpr1^{fl/fl}* mouse lines (**Table 1**). To confirm the specificity of XPR1 towards polyP as the driver of increased platelet procoagulant activity, we characterised platelets from *Xpr1^{fl/fl}* and *Xpr1^{fl/fl} Pf4-Cre* mice. Luminescence assays revealed that intracellular ATP levels were indistinguishable in platelets from *Xpr1^{fl/fl}* and *Xpr1^{fl/fl} Pf4-Cre* mice (not shown). Real time thrombin formation assays and conversion of thrombin substrate S2238 indicated that activated factor X (FXa)-triggered thrombin generation was indistinguishable in PRP from *Xpr1^{fl/fl}* and *Xpr1^{fl/fl} Pf4-Cre* mice (not shown). Moreover, annexin V-staining in flow cytometry showed comparable phosphatidylserine exposure on *Xpr1^{fl/fl} Pf4-Cre,* and *Xpr1^{fl/fl}* mouse platelets upon activation with thrombin and collagen-related peptide (**Supplemental Figure 5A**). CD31, CD41 or CD42b expression was not changed either (**Supplemental Figure 5B - 5D)**. These studies indicate that polyP-independent platelet functions and platelet surface properties are not different between *Xpr1^{fl/fl}* and *Xpr1^{fl/fl} Pf4-Cre* mice. Furthermore, *in vitro* studies demonstrated that aggregation in response to ristocetin (71.7 ± 3.1 *vs.* 69.3 ± 1.4%, *P*=0.45; **Figure 5I**), and low (71.0 ± 5.0 *vs.* 77.0 ± 3.2%, *P*=0.32; **Figure 5J**) or high concentrations of collagen (87.0 ± 2.1 *vs.* 86.5 ± 2.1%, *P*=0.89; **Figure 5K**) was similar in *Xpr1^{fl/fl}* and *Xpr1^{fl/fl} Pf4-Cre* platelets. Consistent with XPR1 inhibition in human platelets (**Figure 4**), thrombus formation on collagen-coated surfaces under arterial and venous shear rates was increased when blood from *Xpr1^{fl/fl} Pf4-Cre* mice was used compared to blood from *Xpr1^{fl/+} Pf4-Cre* and *Xpr1^{fl/fl}* animals (**Supplemental Figure 6**).

Platelet-specific XPR1-deficient mice are prothrombotic

To determine if platelet XPR1 contributes to thrombosis *in vivo*, we challenged platelet-specific XPR1-deficient mice in models of arterial and venous thrombosis. Thrombosis in the carotid artery was induced by topical application of 5% ferric chloride ($FeCl_3$), a

well-established model of platelet-driven thrombus formation [49]. Platelet polyP-induced thrombosis is defective in FXII deficient (*F12$^{-/-}$*) mice [30,42,45,50-52] and consistent with these previous reports, *F12$^{-/-}$* mice were protected from arterial thrombosis as seen by the lack of occlusive thrombi following FeCl$_3$ challenge. Vessel occlusion times were significantly shortened in *Xpr1$^{fl/fl}$ Pf4-Cre* mice compared to *Xpr1$^{fl/fl}$* controls (320 $\pm$ 34 *vs.* 473 $\pm$ 52 s), while occlusion times in heterozygous *Xpr1$^{fl/+}$ Pf4-Cre* mice were almost identical to control mice (472 $\pm$ 50 s, **Figures 6A and 6B**). To study venous thrombosis, we utilized a model of platelet-driven lethal pulmonary thromboembolism (PE). In this assay, platelets were activated by intravenous infusion of collagen/epinephrine and mice that survived beyond 30 minutes were considered survivors (**Figure 6C, lower panel**). In line with earlier data [42,52], *F12$^{-/-}$* mice were largely protected from precipitate disease in this PE model (3/4 animals survived). However, all *Xpr1$^{fl/fl}$ Pf4-Cre* mice (5/5) universally succumbed within the first 3 min after challenge with an average survival time of only 1.1 $\pm$ 0.2 min. Similarly, all *Xpr1$^{fl/fl}$* control mice (5/5) did not survive the collagen/epinephrine challenge but their survival was prolonged by 9-fold (9.8 $\pm$ 1.7 min). Survival times of heterozygous mice were similar to those seen in control mice (9.8 $\pm$ 3.7 min) and 3/7 mice died within the first 5 min of challenge. To confirm PE formation, lung perfusion was studied in all challenged mice using intravenous administration of Evans blue dye. Perfused lung areas turned blue, whereas occluded parts remained their natural pink color. Collagen/epinephrine challenge resulted in almost complete vascular thrombotic occlusion in *Xpr1$^{fl/fl}$ Pf4-Cre* mice visualized by disturbed perfusion of the dye. Heterozygous *Xpr1$^{fl/+}$ Pf4-Cre* and control mice showed incomplete perfusion of the dye indicating partial vessel occlusion. In contrast, lungs of *F12$^{-/-}$* mice presented with uniform distribution of the dye consistent with preserved vessel perfusion (**Figure 6C, upper panel**). Histologic sections from challenged mice showed significantly higher number of large occlusive thrombi per field of view in the lungs of *Xpr1$^{fl/fl}$ Pf4-Cre* mice compared to *Xpr1$^{fl/+}$ Pf4-Cre* and *Xpr1$^{fl/fl}$* mice. Virtually no thrombi were found in challenged *F12$^{-/-}$* mice (**Figure 6D**).

To test whether increased platelet polyP content alters hemostasis, we examined bleeding times and blood loss in *Xpr1$^{fl/fl}$*, *Xpr1$^{fl/fl}$ Pf4-Cre* and *Xpr1$^{fl/+}$ Pf4-Cre* mice. Time to cessation of bleeding after tail clipping was similar in all three groups (90 $\pm$ 15 *vs.* 93 $\pm$ 17 and 128 $\pm$ 17 s, **Figure 6E**). The amount of blood loss as measured by hemoglobin concentration, was also unaltered among respective groups (0.16 $\pm$ 0.05 *vs.* 0.11 $\pm$ 0.03 and 0.25 $\pm$ 0.06; **Figure 6F**). In an independent experimental approach, we monitored bleeding from a tail injury site by gently absorbing blood on a filter paper

without touching the wound. Bleeding times of *Xpr1$^{fl/fl}$*, *Xpr1$^{fl/fl}$ Pf4-Cre* and *Xpr1$^{fl/+}$ Pf4-Cre* mice were recorded over 5 sec intervals and similar to each other (368 ± 8 s, 364 ± 6 s and 372 ± 11 s, **Figure 6G and Supplemental Figure 7**). In sum, these studies indicate that XPR1-deficiency in platelets leads to accumulation of polyP that results in increased thrombosis but has no impact on hemostasis.

DISCUSSION

Our study identifies XPR1 as an instrumental contributor to procoagulant polyP homeostasis in mammalian systems and, by extension, as a key regulator of thrombosis. Specifically, we showed that XPR1 is the most abundant phosphate exporter in platelets and that its expression inversely correlates with polyP content. Increasing intracellular P_i levels by interfering with platelet XPR1 activity leads to polyP accumulation which increases thrombosis risk *in vitro* and *in vivo*, without affecting hemostasis.

Seminal studies have revealed that activated platelets trigger coagulation in a FXII-dependent manner [41,53-55] and work over the last decade identified platelet polyP as a FXII contact activator in human plasma *in vivo* [15]. An array of experimental thrombosis models in mice and baboons confirmed that polyP/FXII-mediated coagulation plays a critical role in arterial and venous thrombo-occlusive diseases [30,52,56-59]. Recently, polyP release and deposition as calcium-rich nanoparticles on the surface of activated platelets has been visualized [16,60]. Consistent with these findings (reviewed in [21,61]), pharmacologic and genetic targeting of platelet XPR1 increased polyP stores and release, increased fibrin formation and accelerated thrombus development under arterial and venous shear rates in human blood (**Figure 4**) and *in vivo* in mice (**Figure 6**). Conversely, mice deficient in inositol hexakisphosphate kinase 1 (IP6K1), a key enzyme implicated in diphosphoinositol pentakisphosphate (IP7, an abundant inositol pyrophosphate) biosynthesis, display lower polyP levels in platelets, lengthened clotting times, altered clot architecture and protection against pulmonary thromboembolism [57]. However, gene disruption of murine *IP6K1* also increases insulin sensitivity, reduces spermatogenesis, and in contrast to platelet XPR1-deficiency (**Figure 6**) compromises hemostasis, indicating the kinase is involved in a multitude of pathways across various tissues [57]. Hermansky-Pudlak syndrome patients also have reduced platelet polyP [62] and as their murine counterparts, FXII-dependent clotting is defective in PRP [15]. In contrast, targeted inhibition of XPR1 led to platelet polyP accumulation and promoted thrombosis (**Figure 3**). Potent agents that neutralize polyP have been developed including cationic polyethylenimine and polyamidoamine dendrimers [56], crown ether-based universal heparin reversal agents (UHRAs) [59], and exopolyphosphatase mutants that either degrade (PPX) or bind (PPX_Δ12) the polymer [30]. These polyP inhibitors interfere with platelet-driven arterial and venous thrombosis but they spare hemostasis, evidenced by their limited impact on bleeding [30,59]. This selective role of polyP inhibitors on thrombosis is in line with our findings that polyP accumulation in XPR1-defective platelets differentially contributes to thrombosis

whilst sparing platelet hemostatic functions (**Figures 3, 4, 6**). Thromboprotection in the absence of bleeding conferred by various polyP inhibitors also supports the notion that platelet polyP contributes to coagulation *in vivo* in large part, through FXII activation. In contrast to other potential polyP targets including coagulation factors V and XI, tissue factor pathway inhibitor (TFPI), von Willebrand factor or fibrinolytic pathway components [17-20,22,63,64], FXII has no role in hemostatic coagulation mechanisms and thus interference with its activation does not increase bleeding.

PolyP is an evolutionary ancient molecule that serves as a storage form for P_i. The role of P_i for polyP synthesis and the function of P_i export in the regulation of polyP is evolutionarily conserved from prokaryotes to eukaryotes [27]. In prokaryotes the conversion of P_i to polyP contributes to reducing intracellular osmotic pressure [1], however it is unknown whether this function is preserved in higher eukaryotic cells. P_i transporters help maintain intracellular P_i concentration at significantly higher levels than extracellular P_i (60 – 100 mM *vs.* 1 mM). Disturbance of P_i levels affects polyP content in HEK293 cells and similarly, influences the XPR1-regulated P_i/polyP equilibrium in megakaryocytes and platelets (**Figures 2, 5**). XPR1 expression in *Pf4-Cre Xpr1^fl/fl* mouse platelets was below residual XPR1 levels in cultured megakaryocytes from these mice. These higher XPR1 levels might be due to XPR1 expressing cells in the primary megakaryocyte preparation and incomplete Cre-mediated *Xpr1* ablation (**Figures 5**). P_i transporter activity controls P_i/polyP levels in bacteria and yeast [6,8,27,65]. While an association of P_i accumulation and storage as polyP seems to be conserved from prokaryotes to metazoans, regulation of polyP metabolism in mammalians has remained enigmatic [1]. XPR1 activity is regulated involving the phosphate-sensing domain SPX which responds to P_i levels [66]. Moreover, XPR1 trafficking to distinct subcellular compartments (**Figure 1E**) [67], restricts its impact on intracellular polyP content to specific locations and pools within cells [16, 30]. Indeed, targeting *IP6K1* reduced platelet polyP levels by about 50% [57], supporting that polyP accumulation occurs in specific sites within cells and in an orderly, regulated manner.

Beyond its role in platelets, impaired XPR1 function due to missense mutations in humans has been linked to an adult-onset neurodegenerative disease, primary familial brain calcification (PFBC). Although PFBC is a rare disorder characterized by calcium-(poly)phosphate deposits in the basal ganglia and other brain regions [68,69], its clinical phenotype highlights the impact of P_i/polyP regulation in health and disease. Consistently, the number of missense variants in the human *XPR1* gene is far below the number of expected variants with a significantly increased Z-score of 3.23 (https://gnomad.broadinstitute.org/) further confirming its vital role in homeostasis.

In sum, our data indicate that the ancient link between intracellular P_i and polyP levels is conserved in mammals. Consistent with their functions in prokaryotes, P_i-transporters also regulate polyP homeostasis in platelets and influence thrombosis.

ACKNOWLEDGMENTS

AUTHORSHIP CONTRIBUTION

S.G., E.X.S., C.M. and T.R. conceived and/or designed the study. L.B and J.O. provided the bioinformatics. R.K.M., M.A., G.P. and M.H. performed *in vitro* experiments and R.K.M. performed the *in vivo* studies. M.S. performed the TEM analyses. D.F. provided the *in vivo* model. C.D., A.S., T.H., M.F., M.G., S.R.J., S.B. and C.K. conceived and discussed data. R.K.M., M.A, E.X.S. and T.R. wrote the manuscript. All authors edited the manuscript.

DISCLOSURE OF CONFLICTS OF INTEREST

The authors declare no competing financial interests.

REFERENCES

1.   Rao NN, Gomez-Garcia MR, Kornberg A. Inorganic polyphosphate: essential for growth and survival. *Annu Rev Biochem*. 2009;78:605-647.

2.   Igor S. Kulaev VV, Tatiana Kulakovskaya. The Biochemistry of Inorganic Polyphosphates (ed 2nd). Chichester: John Wiley & Sons; 2004.

3.   Achbergerova L, Nahalka J. Polyphosphate--an ancient energy source and active metabolic regulator. *Microb Cell Fact*. 2011;10:63.

4.   Xie L, Jakob U. Inorganic polyphosphate, a multifunctional polyanionic protein scaffold. *J Biol Chem*. 2019;294(6):2180-2190.

5.   Secco D, Wang C, Shou H, Whelan J. Phosphate homeostasis in the yeast Saccharomyces cerevisiae, the key role of the SPX domain-containing proteins. *FEBS Lett*. 2012;586(4):289-295.

6.   Hurlimann HC, Stadler-Waibel M, Werner TP, Freimoser FM. Pho91 Is a vacuolar phosphate transporter that regulates phosphate and polyphosphate metabolism in Saccharomyces cerevisiae. *Mol Biol Cell*. 2007;18(11):4438-4445.

7.   Freimoser FM, Hurlimann HC, Jakob CA, Werner TP, Amrhein N. Systematic screening of polyphosphate (poly P) levels in yeast mutant cells reveals strong interdependence with primary metabolism. *Genome Biol*. 2006;7(11):R109.

8.   Vagabov VM, Trilisenko LV, Kulaev IS. Dependence of inorganic polyphosphate chain length on the orthophosphate content in the culture medium of the yeast Saccharomyces cerevisiae. *Biochemistry (Mosc)*. 2000;65(3):349-354.

9.   Pestov NA, Kulakovskaya TV, Kulaev IS. Inorganic polyphosphate in mitochondria of Saccharomyces cerevisiae at phosphate limitation and phosphate excess. *FEMS Yeast Res*. 2004;4(6):643-648.

10.   Docampo R, Moreno SN. Acidocalcisomes. *Cell Calcium*. 2011;50(2):113-119.

11.   Deinema MH, van Loosdrecht M, Scholten A. Some physiological characteristics of Acinetobacter spp. accumulating large amounts of phosphate. *Wat Sci Technol*. 1985;17:119–125.

12.   Moreno-Sanchez D, Hernandez-Ruiz L, Ruiz FA, Docampo R. Polyphosphate is a novel pro-inflammatory regulator of mast cells and is located in acidocalcisomes. *J Biol Chem*. 2012;287(34):28435-28444.

13.   Holmstrom KM, Marina N, Baev AY, Wood NW, Gourine AV, Abramov AY. Signalling properties of inorganic polyphosphate in the mammalian brain. *Nat Commun*. 2013;4:1362.

14. Ruiz FA, Lea CR, Oldfield E, Docampo R. Human platelet dense granules contain polyphosphate and are similar to acidocalcisomes of bacteria and unicellular eukaryotes. *J Biol Chem*. 2004;279(43):44250-44257.

15. Muller F, Mutch NJ, Schenk WA, et al. Platelet polyphosphates are proinflammatory and procoagulant mediators in vivo. *Cell*. 2009;139(6):1143-1156.

16. Verhoef JJ, Barendrecht AD, Nickel KF, et al. Polyphosphate nanoparticles on the platelet surface trigger contact system activation. *Blood*. 2017;129(12):1707-1717.

17. Montilla M, Hernandez-Ruiz L, Garcia-Cozar FJ, Alvarez-Laderas I, Rodriguez-Martorell J, Ruiz FA. Polyphosphate binds to human von Willebrand factor in vivo and modulates its interaction with glycoprotein Ib. *J Thromb Haemost.* 2012;10(11):2315-2323.

18. Morrissey JH, Smith SA. Polyphosphate as modulator of hemostasis, thrombosis, and inflammation. *J Thromb Haemost*. 2015;13 Suppl 1:S92-97.

19. Puy C, Tucker EI, Ivanov IS, et al. Platelet-Derived Short-Chain Polyphosphates Enhance the Inactivation of Tissue Factor Pathway Inhibitor by Activated Coagulation Factor XI. *PLoS One*. 2016;11(10):e0165172.

20. Mutch NJ. Polyphosphate as a haemostatic modulator. *Biochem Soc Trans*. 2016;44(1):18-24.

21. Weitz JI, Fredenburgh JC. Platelet polyphosphate: the long and the short of it. *Blood*. 2017;129(12):1574-1575.

22. Baker CJ, Smith SA, Morrissey JH. Polyphosphate in thrombosis, hemostasis, and inflammation. *Res Pract Thromb Haemost*. 2019;3(1):18-25.

23. Mailer RKW, Hanel L, Allende M, Renne T. Polyphosphate as a Target for Interference With Inflammation and Thrombosis. *Front Med (Lausanne)*. 2019;6:76.

24. Battini JL, Rasko JE, Miller AD. A human cell-surface receptor for xenotropic and polytropic murine leukemia viruses: possible role in G protein-coupled signal transduction. *Proc Natl Acad Sci U S A*. 1999;96(4):1385-1390.

25. Wege S, Poirier Y. Expression of the mammalian Xenotropic Polytropic Virus Receptor 1 (XPR1) in tobacco leaves leads to phosphate export. *FEBS Lett*. 2014;588(3):482-489.

26. Giovannini D, Touhami J, Charnet P, Sitbon M, Battini JL. Inorganic phosphate export by the retrovirus receptor XPR1 in metazoans. *Cell Rep*. 2013;3(6):1866-1873.

27. Jimenez V, Docampo R. TcPho91 is a contractile vacuole phosphate sodium symporter that regulates phosphate and polyphosphate metabolism in Trypanosoma cruzi. *Mol Microbiol*. 2015;97(5):911-925.

28. Ansermet C, Moor MB, Centeno G, et al. Renal Fanconi Syndrome and Hypophosphatemic Rickets in the Absence of Xenotropic and Polytropic Retroviral Receptor in the Nephron. *J Am Soc Nephrol*. 2017;28(4):1073-1078.

29. Nickel KF, Ronquist G, Langer F, et al. The polyphosphate-factor XII pathway drives coagulation in prostate cancer-associated thrombosis. *Blood*. 2015;126(11):1379-1389.

30. Labberton L, Kenne E, Long AT, et al. Neutralizing blood-borne polyphosphate in vivo provides safe thromboprotection. *Nat Commun*. 2016;7:12616.

31. Levi M, Gratton E, Forster IC, et al. Mechanisms of phosphate transport. *Nat Rev Nephrol*. 2019;15(8):482-500.

32. Boyanova D, Nilla S, Birschmann I, Dandekar T, Dittrich M. PlateletWeb: a systems biologic analysis of signaling networks in human platelets. *Blood*. 2012;119(3):e22-34.

33. Amisten S, Braun OO, Bengtsson A, Erlinge D. Gene expression profiling for the identification of G-protein coupled receptors in human platelets. *Thromb Res*. 2008;122(1):47-57.

34. Lewandrowski U, Wortelkamp S, Lohrig K, et al. Platelet membrane proteomics: a novel repository for functional research. *Blood*. 2009;114(1):e10-19.

35. Rangarajan ES, Nadeau G, Li Y, et al. The structure of the exopolyphosphatase (PPX) from Escherichia coli O157:H7 suggests a binding mode for long polyphosphate chains. *J Mol Biol*. 2006;359(5):1249-1260.

36. Battini JL, Danos O, Heard JM. Receptor-binding domain of murine leukemia virus envelope glycoproteins. *J Virol*. 1995;69(2):713-719.

37. Fass D, Kim PS. Dissection of a retrovirus envelope protein reveals structural similarity to influenza hemagglutinin. *Curr Biol*. 1995;5(12):1377-1383.

38. Yan Y, Liu Q, Wollenberg K, Martin C, Buckler-White A, Kozak CA. Evolution of functional and sequence variants of the mammalian XPR1 receptor for mouse xenotropic gammaretroviruses and the human-derived retrovirus XMRV. *J Virol*. 2010;84(22):11970-11980.

39. Kozak CA. Susceptibility of wild mouse cells to exogenous infection with xenotropic leukemia viruses: control by a single dominant locus on chromosome 1. *J Virol*. 1985;55(3):690-695.

40.   Zhu S, Herbig BA, Yu X, Chen J, Diamond SL. Contact Pathway Function During Human Whole Blood Clotting on Procoagulant Surfaces. *Front Med (Lausanne)*. 2018;5:209.

41.   Walsh PN, Griffin JH. Contributions of human platelets to the proteolytic activation of blood coagulation factors XII and XI. *Blood*. 1981;57(1):106-118.

42.   Renne T, Pozgajova M, Gruner S, et al. Defective thrombus formation in mice lacking coagulation factor XII. *J Exp Med*. 2005;202(2):271-281.

43.   Smith SA, Mutch NJ, Baskar D, Rohloff P, Docampo R, Morrissey JH. Polyphosphate modulates blood coagulation and fibrinolysis. *Proc Natl Acad Sci U S A*. 2006;103(4):903-908.

44.   Larsson M, Rayzman V, Nolte MW, et al. A factor XIIa inhibitory antibody provides thromboprotection in extracorporeal circulation without increasing bleeding risk. *Sci Transl Med*. 2014;6(222):222ra217.

45.   Hagedorn I, Schmidbauer S, Pleines I, et al. Factor XIIa inhibitor recombinant human albumin Infestin-4 abolishes occlusive arterial thrombus formation without affecting bleeding. *Circulation*. 2010;121(13):1510-1517.

46.   van der Meijden PE, Munnix IC, Auger JM, et al. Dual role of collagen in factor XII-dependent thrombus formation. *Blood*. 2009;114(4):881-890.

47.   Kleinschnitz C, Stoll G, Bendszus M, et al. Targeting coagulation factor XII provides protection from pathological thrombosis in cerebral ischemia without interfering with hemostasis. *J Exp Med*. 2006;203(3):513-518.

48.   Labberton L, Long AT, Gendler SJ, et al. A Flow Cytometry-Based Assay for Procoagulant Platelet Polyphosphate. *Cytometry B Clin Cytom*. 2018;94(2):369-373.

49.   Eckly A, Hechler B, Freund M, et al. Mechanisms underlying FeCl3-induced arterial thrombosis. *J Thromb Haemost*. 2011;9(4):779-789.

50.   Cheng Q, Tucker EI, Pine MS, et al. A role for factor XIIa-mediated factor XI activation in thrombus formation in vivo. *Blood*. 2010;116(19):3981-3989.

51.   von Bruhl ML, Stark K, Steinhart A, et al. Monocytes, neutrophils, and platelets cooperate to initiate and propagate venous thrombosis in mice in vivo. *J Exp Med*. 2012;209(4):819-835.

52.   Stavrou EX, Fang C, Merkulova A, et al. Reduced thrombosis in Klkb1-/- mice is mediated by increased Mas receptor, prostacyclin, Sirt1, and KLF4 and decreased tissue factor. *Blood*. 2015;125(4):710-719.

53.   Castaldi PA, Larrieu MJ, Caen J. Availability of platelet Factor 3 and activation of factor XII in thrombasthenia. *Nature*. 1965;207(995):422-424.

54. Johne J, Blume C, Benz PM, et al. Platelets promote coagulation factor XII-mediated proteolytic cascade systems in plasma. *Biol Chem*. 2006;387(2):173-178.

55. Back J, Sanchez J, Elgue G, Ekdahl KN, Nilsson B. Activated human platelets induce factor XIIa-mediated contact activation. *Biochem Biophys Res Commun*. 2010;391(1):11-17.

56. Smith SA, Choi SH, Collins JN, Travers RJ, Cooley BC, Morrissey JH. Inhibition of polyphosphate as a novel strategy for preventing thrombosis and inflammation. *Blood*. 2012;120(26):5103-5110.

57. Ghosh S, Shukla D, Suman K, et al. Inositol hexakisphosphate kinase 1 maintains hemostasis in mice by regulating platelet polyphosphate levels. *Blood*. 2013;122(8):1478-1486.

58. Matafonov A, Leung PY, Gailani AE, et al. Factor XII inhibition reduces thrombus formation in a primate thrombosis model. *Blood*. 2014;123(11):1739-1746.

59. Travers RJ, Shenoi RA, Kalathottukaren MT, Kizhakkedathu JN, Morrissey JH. Nontoxic polyphosphate inhibitors reduce thrombosis while sparing hemostasis. *Blood*. 2014;124(22):3183-3190.

60. Wijeyewickrema LC, Lameignere E, Hor L, et al. Polyphosphate is a novel cofactor for regulation of complement by a serpin, C1 inhibitor. *Blood*. 2016;128(13):1766-1776.

61. Nickel KF, Long AT, Fuchs TA, Butler LM, Renne T. Factor XII as a Therapeutic Target in Thromboembolic and Inflammatory Diseases. *Arterioscler Thromb Vasc Biol*. 2017;37(1):13-20.

62. Huizing M, Helip-Wooley A, Westbroek W, Gunay-Aygun M, Gahl WA. Disorders of lysosome-related organelle biogenesis: clinical and molecular genetics. *Annu Rev Genomics Hum Genet*. 2008;9:359-386.

63. Choi SH, Smith SA, Morrissey JH. Polyphosphate accelerates factor V activation by factor XIa. *Thromb Haemost*. 2015;113(3):599-604.

64. Mutch NJ, Engel R, Uitte de Willige S, Philippou H, Ariens RA. Polyphosphate modifies the fibrin network and down-regulates fibrinolysis by attenuating binding of tPA and plasminogen to fibrin. *Blood*. 2010;115(19):3980-3988.

65. Shirahama K, Yazaki Y, Sakano K, Wada Y, Ohsumi Y. Vacuolar function in the phosphate homeostasis of the yeast Saccharomyces cerevisiae. *Plant Cell Physiol*. 1996;37(8):1090-1093.

66. Wild R, Gerasimaite R, Jung JY, et al. Control of eukaryotic phosphate homeostasis by inositol polyphosphate sensor domains. *Science*. 2016;352(6288):986-990.

67. Tello-Lafoz M, Martinez-Martinez G, Rodriguez-Rodriguez C, et al. Sorting nexin 27 interactome in T-lymphocytes identifies zona occludens-2 dynamic redistribution at the immune synapse. *Traffic*. 2017;18(8):491-504.

68. Legati A, Giovannini D, Nicolas G, et al. Mutations in XPR1 cause primary familial brain calcification associated with altered phosphate export. *Nat Genet*. 2015;47(6):579-581.

69. Guo XX, Zou XH, Wang C, et al. Spectrum of SLC20A2, PDGFRB, PDGFB, and XPR1 mutations in a large cohort of patients with primary familial brain calcification. *Hum Mutat*. 2019;40(4):392-403.

TABLE 1. **Blood counts in *Xpr1^{fl/fl}*, *Xpr1^{fl/fl} Pf4-Cre* and *Xpr1^{fl/+} Pf4-Cre* murine blood samples.**

	Xpr1^{fl/fl} (n = 9)	Xpr1^{fl/fl} Pf4-Cre (n = 11)	Xpr1^{fl/+} Pf4-Cre (n = 18)	p
RBC (M/μL)	9.40±1.17	9.73±0.61	9.31±0.93	0.43
HGB (g/dL)	14.24±1.69	14.61±0.75	13.81±1.09	0.53
HCT (%)	47.66±7.03	49.33± 3.45	46.86± 5.36	0.50
MCV (fL)	50.55±01.87	50.71±1.70	50.30± 1.68	0.85
MCH (pg)	15.18±0.49	15.04± 0.40	14.88±0.47	0.48
MCHC (g/dL)	30.03±1.32	29.67± 1.19	29.61± 0.47	0.53
RDW-SD (fL)	29.62±2.22	29.10± 1.74	30.24±1.89	0.55
RDW-CV (%)	22.76±2.08	23.02±1.19	23.07± 1.63	0.72
RET (K/μL)	379.41±111.22	386.60± 97.83	355.38± 82.14	0.88
RET (%)	4.01±0.93	3.97± 0.97	3.82± 0.80	0.92
PLT (K/μL)	607.67±266.56	717.54± 347.24	757.17±300.98	0.44
PDW (fL)	7.21±0.80	7.20± 0.40	6.96± 0.86	0.97
MPV (fL)	6.36±0.43	6.23± 0.38	6.05± 0.52	0.49
P-LCR (%)	5.03±2.39	3.59± 1.11	3.55± 2.14	0.09
PCT (%)	0.37±0.19	0.45± 0.22	0.46± 0.18	0.38
WBC (K/μL)	6.22±4.71	6.96±3.53	6.73± 4.11	0.69
NEUT (K/μL)	0.86± 0.90	1.18± 0.91	0.95± 1.02	0.44
LYMPH (K/μL)	5.14±3.96	5.56±3.06	5.56± 3.25	0.79
MONO (K/μL)	0.11±0.13	0.12± 0.06	0.09± 0.05	0.80
EO (K/μL)	0.11±0.08	0.09± 0.08	0.12± 0.12	0.50
BASO (K/μL)	0.00±0.00	0.01 ± 0.01	0.00± 0.01	n/a
NEUT (%)	13.8±10.1	17.0 ± 12.4	12.8 ± 7.0	0.54
LYMPH (%)	82.7 ±11.0	79.9 ± 12.3	83.8 ± 7.4	0.60
MONO (%)	1.7 ± 0.9	2.0 ± 1.1	1.7 ± 1.4	0.54
EO (%)	1.87± 0.79	1.08 ± 0.61	1.69± 1.03	0.2
BASO (%)	0.01± 0.03	0.07± 0.10	0.07± 0.15	n/a

p values represent comparisons between *Xpr1^{fl/fl} Pf4-Cre vs. Xpr1^{fl/fl}* murine blood counts. Mean ± SD.

Abbreviations: RBC, red blood cells; HGB, hemoglobin; HCT, hematocrit; MCV, mean corpuscular volume; MCH, mean corpuscular hemoglobin, MCHC, mean corpuscular hemoglobin concentration, RDW-SD, red cell distribution width standard deviation; RDW-CV, red cell distribution coefficient of variation; RET, reticulocytes; PLT, platelets; PDW, platelet distribution width; MPV, mean platelet volume; P-LCR, platelet large cell ratio; PCT, plateletcrit; WBC, white blood cells; NEUT, neutrophils, LYMPH, lymphocytes; MONO, monocytes; EO, eosinophils; BASO, basophils; n/a, not applicable as the absolute number of events counted was too low to perform statistics.

FIGURE LEGENDS

FIGURE 1. XPR1 is a major phosphate transporter on platelets.

(**A**) Data from the Human Protein Atlas (HPA) project (https://www.proteinatlas.org/) and GTEx Analysis V7 (https://gtexportal.org) were used to determine the expression of transcripts encoding for the ten reported phosphate transporters in bone marrow and whole blood, respectively. Platelet web (http://plateletweb.bioapps.biozentrum.uni-wuerzburg.de/plateletweb.php) and PubMed were used to establish if protein expression on platelets was previously described. Transcripts Per Million (TPM); Fragments Per Kilobase of exon model per Million reads mapped (FPKM). Cell membranes from indicated numbers of (**B**) human or (**C**) mouse platelets were analyzed by western blotting using antibodies directed against the XPR1 N-terminal or C-terminal portions. Lysed HEK293 cells transiently transfected with a pCHIX-XPR1 coding plasmid were loaded as a positive control (XPR1). (**D**) Bright field image (left panel) and confocal laser scanning image (middle panel, green) of XPR1 staining in non-permeabilized resting human platelets. The right panel shows the merged image. Scale: 1 μm. (**E**) Transmission electron microscopy (TEM) of immunogold- (10 nm particles) stained XPR1 on human platelets. Open canalicular system (OCS), dense tubular system (DTS) and α-granules are shown. Arrows indicate XPR1, scale bar: 100 nm.

FIGURE 2. XPR1 expression levels inversely correlate with polyP content in cells.

HEK293 cells and MEG-01 megakaryocytes were transiently transfected with indicated amounts of pCHIX-XPR1 or empty (Mock) vector. (**A**) HEK293 and (**B**) MEG-01 cells were analyzed by western blotting with anti-XPR1 antibodies (upper panels) after 24 and 48 h, respectively. The cytoskeleton protein vasodilator-stimulated phosphoprotein (VASP) served as loading control (lower panels). XPR1 (blue columns) and polyP (red columns) levels in XPR1-overexpressing (**C**) HEK293 and (**D**) MEG-01 cells. HEK293 (**E**) or MEG-01 (**F**) cells were transfected with 250 nM *XPR1* siRNA and *XPR1* mRNA expression (blue columns) and polyP (red columns) were analyzed every 24 h for 5 days. Expression of *XPR1* mRNA was normalized to 18S rRNA signal and blotted as percentage of *XPR1* expression at day 0 following control siRNA treatment (100%). Data are expressed as mean ± SEM, one-way ANOVA and Tukey's multiple comparison test; * $P<0.05$; ** $P<0.01$. PolyP from (**G**) XPR1-overexpressing (OE) or (**H**) siRNA-treated *XPR1* knock-down (KD) cells was

extracted, equal amounts (10 ng)/lane polyP were loaded, separated on polyacrylamide/urea gel, and visualized by DAPI negative staining. For control, purified polyP was loaded before (-) or after (+) incubation with exopolyphosphatase (PPX, 10 µg ml^{-1} for 1 h).

FIGURE 3. Interference with XPR1 increases platelet polyP and promotes activated platelet-driven coagulation via the polyP/FXII pathway.

(**A-B**) Washed human platelets were pre-incubated with (**A**) xenotropic virus-derived ligand (XVDL), (**B**) polytropic virus-derived ligand (PVDL) or (**C**) XVDL (200 µg ml^{-1}) and increasing PVDL concentrations (0-600 µg ml^{-1}) for 1, 4, 8 or 24 h. PolyP was measured as monophosphate using malachite green assay. PolyP content before treatment was set to 100%. Analysis of released (**D-E**) soluble polyP in the supernatant and (**F-G**) insoluble platelet membrane-associated polyP in collagen-stimulated (10 µg ml^{-1}) platelets following a 4 h incubation with XVDL or PVDL, respectively. PolyP was measured as above. (**H-I**) Real-time thrombin formation in collagen-stimulated human platelet rich plasma (PRP) that was pre-incubated for 4 h with XVDL or PVDL (2 – 200 µg ml^{-1}). Representative experiment of *n*=5 is shown. (**J**) Endogenous thrombin potential (ETP) and (**K**) maximum (peak) thrombin triggered in collagen-stimulated human platelet rich plasma pre-incubated for 4 h with XVDL (200 µg ml^{-1}) in the presence of PPX (500 µg ml^{-1}), PPX_Δ12 (500 µg ml^{-1}), 3F7 (650 nM) or infestin-4 (500 µg ml^{-1}). Data are expressed as mean ± SEM; *n*=3; n.s. non-significant; * *P*<0.05; ** *P*<0.01.

FIGURE 4. Targeting XPR1 promotes thrombus formation in blood under flow.

Citrated human whole blood pre-incubated with XVDL (2 - 200 µg ml^{-1}, 4 h) or PPX (2 mg ml^{-1}, 30 min) was readjusted to physiological Ca^{2+} and Mg^{2+} concentrations and perfused for 4 min over collagen-coated surface at an arterial (1000 s^{-1}, **A**) or venous (100 s^{-1}, **B**) shear rate. Upper panels: representative phase-contrast images of thrombi formed during perfusion following incubation with indicated XVDL concentrations. Scale: 10 µm. Bar graphs indicate the percentage of surface area covered by thrombi. Mean ± SD, *n*=3. Comparisons were performed using one-way ANOVA and Tukey's multiple comparison test; * *P*<0.05, ** *P*<0.01. (**C-D**) Representative bright-field images and immunofluorescence microscopy of thrombi formed at t = 4 min under arterial (**C**) or venous (**D**) flow. Staining for fibrin (59D8, green), platelets (GPIb, red) and merged images are shown. Scale: 10 µm. (**E-F**) Bright-field images and

immunofluorescence microscopy of thrombi formed at t = 4 min under arterial (**E**) or venous (**F**) flow. Representative images of *n*=6 individual experiments. Scale: 10 µm. PolyP signal (PPX_Δ12, green) was quantified from 4 randomly selected high-power images by ImageJ. Data were statistically analyzed using Student's t-test; ** *P*<0.01.

FIGURE 5. PolyP is increased in platelet XPR1-deficient mice.

(**A**) Genotyping results of *Xpr1^{fl/fl}*, *Xpr1^{fl/+}* *Pf4-Cre* and *Xpr1^{fl/fl}* *Pf4-Cre* mice. (**B**) Relative *Xpr1* mRNA expression levels in megakaryocytes enriched from cultured bone marrow cells of *Xpr1^{fl/fl}* and *Xpr1^{fl/fl}* *Pf4-Cre* mice. (**C**) XPR1 signal in megakaryocyte-enriched bone marrow cell cultures of *Xpr1^{fl/fl}* and *Xpr1^{fl/fl}* *Pf4-Cre* mice measured by flow cytometry. SSC is sideward scatter. Numbers in the upper right corner provide the portion of gated cells. Megakaryocyte preparations derived from two *Xpr1^{fl/fl}* and *Xpr1^{fl/fl}* *Pf4-Cre* mice each analyzed for XPR1 content by western blotting. β-actin served as loading control (lower panels). (**D**) *Xpr1* mRNA expression in platelets of *Xpr1^{fl/fl}* and *Xpr1^{fl/fl}* *Pf4-Cre* mice. *Xpr1* expression in *Xpr1^{fl/fl}* mouse platelets is set to 100%. (**E**) Plasma membranes isolated from 10^9 platelets of *Xpr1^{fl/fl}*, *Xpr1^{fl/fl}* *Pf4-Cre* or *Xpr1^{fl/+}* *Pf4-Cre* mice were analyzed by western blotting using antibodies directed against the XPR1 N-terminus. β-actin served as loading control. (**F**) Total polyP in platelets of *Xpr1^{fl/fl}*, *Xpr1^{fl/fl}* *Pf4-Cre* or *Xpr1^{fl/+}* *Pf4-Cre* mice. Soluble polyP (**G**) and membrane-associated polyP (**H**) released by collagen-stimulated platelets measured as monophosphate in PPX-treated (50 µg ml^{-1}, 1 h) platelet supernatants. Symbols represent individual mice, one-way ANOVA and Tukey's multiple comparison test was performed for statistical analysis; * *P*<0.05, ** *P*<0.01. Platelet aggregation following activation by (**I**) 1.5 µg ml^{-1} ristocetin, and (**J**) 5 or (**K**) 10 µg ml^{-1} collagen at 10 min. Transmission of suspended resting platelets is 0% and buffer 100%. Data were analyzed by Student's t-test; n.s. non-significant.

FIGURE 6. Increased arterial and venous thrombosis but normal hemostasis in platelet XPR1 deficient mice.

(**A**) Thrombus formation was induced in the left carotid artery by topical application of 5% FeCl$_3$ for 3 min in *F12^{-/-}*, *Xpr1^{fl/fl}*, *Xpr1^{fl/+}* *Pf4-Cre* and *Xpr1^{fl/fl}* *Pf4-Cre* mice. Artery patency was monitored by a flow probe until complete occlusion occurred and zero flow was recorded for >10 min. Representative curves for *n*=5-8 mice/genotype. (**B**) Time to complete carotid artery occlusion in *Xpr1^{fl/fl}*, *Xpr1^{fl/fl}* *Pf4-Cre* and *Xpr1^{fl/+}* *Pf4-Cre* mice from (A). (**C**) Pulmonary thromboembolism was induced by intravenous

infusion of collagen & epinephrine in $Xpr1^{fl/fl}$, $Xpr1^{fl/fl}$ *Pf4-Cre*, $Xpr1^{fl/+}$ *Pf4-Cre* and $F12^{-/-}$ mice. Shortly after the onset of respiratory arrest, or at 30 min for mice that survived collagen-epinephrine treatment, Evans blue was intravenously infused while the heart was still beating. Occluded parts of the lungs remained their natural pinkish color. Lungs were excised and perfusion defects were analyzed by impaired distribution of the dye in lung tissue (upper panel). Scale: 5 mm. Survival time was assessed (lower panel). (**D**) Hematoxylin and eosin stained sections of lungs from $Xpr1^{fl/fl}$, $Xpr1^{fl/fl}$ *Pf4-Cre*, $Xpr1^{fl/+}$ *Pf4-Cre* and $F12^{-/-}$ mice 30 min after collagen-epinephrine challenge (upper panels). The number of thrombi per visual field was counted at 10x magnification from *n*=6 individual mice (lower panels). Data represent mean ± SD of 10 fields each. Green asterisks mark thrombi. Scale: 100 μm. Bleeding times and blood loss from clipped tails assessed the hemostatic capacity of $Xpr1^{fl/fl}$, $Xpr1^{fl/fl}$ *Pf4-Cre*, $Xpr1^{fl/+}$ *Pf4-Cre* mice. (**E**) Bleeding time and (**F**) total hemoglobin loss as determined by absorbance of hemoglobin in 37°C phosphate buffered saline at λ=575 nm. (**G**) Tail bleeding times were analyzed by gently adsorbing blood with a filter paper. Each symbol represents one individual animal, ** $P < 0.01$, * $P < 0.05$, n.s. non-significant by one-way ANOVA and Tukey's multiple comparison test.

SUPPLEMENTAL DATA

XENOTROPIC AND POLYTROPIC RETROVIRUS RECEPTOR 1 REGULATES PROCOAGULANT PLATELET POLYPHOSPHATE

Reiner K. Mailer, Mikel Allende, Marco Heestermans, Michaela Schweizer, Carsten Deppermann, Maike Frye, Giordano Pula, Jacob Odeberg, Mathias Gelderblom, Stefan Rose-John, Albert Sickmann, Stefan Blankenberg, Tobias Huber, Christian Kubisch, Coen Maas, Stepan Gambaryan, Dmitri Firsov, Evi X. Stavrou, Lynn Butler, Thomas Renné

SUPPLEMENTAL METHODS

Pulmonary thrombosis model

As described previously [1], mice were anesthetized by intraperitoneal injection of ketamine (120 mg kg^{-1} BW) and xylazine (16 mg kg^{-1} BW) in saline (10 ml kg^{-1} BW). Horm collagen (200 μg kg^{-1} BW) was mixed with epinephrine (60 μg kg^{-1} BW) and slowly injected into the inferior vena cava. Animals surviving the challenge for >30 min were considered survivors. After the onset of respiratory arrest and while the heart was still beating or after 30 min for those animals that survived, Evans blue dye (1% in 0.9% saline) was retroorbitally injected to assess lung perfusion [2]. Lungs were excised and photographed.

Arterial thrombosis model

Ferric Chloride (FeCl$_3$)-induced arterial thrombosis was performed as previously published [1,3] with minor modifications. In brief, mice were anesthetized by isoflurane inhalation, a segment of the carotid artery was exposed, and a flow probe size 0.5 (Transonic) was inserted around the artery to monitor blood flow. Thrombus formation was induced by topically applying a piece of Whatman filter paper (1 × 1.5 mm) saturated with 5% FeCl$_3$. After 3 min, the filter paper was removed and blood flow was continuously recorded until it reached 0 ml min^{-1} for >10 min.

Electron microscopy

Washed human platelets were fixed with 0.1% wt/vol glutaraldehyde and 4% wt/vol paraformaldehyde in PBS, pH 7.2 for 2 hours. Following fixation, cells were washed several times in PBS and centrifuged at 1,000 g after each washing step. For post-embedding immunogold labeling, small pieces of cryoprotected cell pellets (in 2.3 M sucrose) were mounted on specimen holders and immersed in liquid nitrogen. Ultrathin sections (60 nm)

were cut and labeled, as described previously [4]. Sections were collected on Carbon-Formvar-coated copper grids (Science Services, Germany). An antibody against XPR1 (14174-1-AP, Proteintech) (1:50) was recognized with Protein A coupled to 10 nm colloidal gold particles (G. Posthuma, University Medical Center Utrecht). Sections were analyzed in an EM902 transmission electron microscope (Zeiss, Germany). Image acquisition was performed using a TRS 2K digital camera (A. Tröndle, Moorenweis, Germany).

Cell culture

HEK293 cells were grown on poly-D-lysine-coated 6-well plates in Dulbecco´s modified eagle medium (DMEM; Thermo Scientific) with 10% fetal bovine serum (FBS; Thermo Scientific) and 1% penicillin/streptomycin (Thermo Scientific). MEG-01 cells were grown in RPMI-1640 medium (Thermo Scientific) supplemented with 10% FBS and 1% penicillin/streptomycin.

Megakaryocyte enrichment from bone marrow cell cultures

Bone marrow from *Xpr1*$^{fl/fl}$ and *Xpr1*$^{fl/fl}$ *Pf4-Cre* mice was flushed from the tibias and femurs with ice cold PBS using a 10 ml syringe and 26 G needle. Bone marrow cell clumps were then flushed using a new 10 ml syringe and 18 G, 22 G and 26 G needles to obtain a single cell suspension. The suspension was passed through a 100 µm filter and cultured in StemPro medium (Gibco) supplemented with StemPro nutrient supplement, L-glutamine, penicillin/streptomycin and 50 ng/ml stem cell factor (SCF, R&D Systems) at 37°C 5% CO_2. On day 2, cells were washed (200 *g*, 5 min, RT), resuspended in modified StemPro medium and cultured for another 2 days. On day 4, cells were washed (200 *g*, 5 min, room temperature) and layered on top of a 1.5 - 3% BSA in a PBS gradient. Megakaryocytes were allowed to sediment at 37°C, 5% CO_2. After 30 min, the gradient was carefully removed to isolate the megakaryocyte pellet [5].

Flow cytometry

Megakaryocytes prepared from bone marrow of *Xpr1*$^{fl/f}$ and *Xpr1*$^{fl/fl}$ *Pf4-Cre* mice were stained for CD41 (clone: MWReg30, Biolegend; 1:20 dilution) and CD42b (clone: Xia.G5, Emfret Analytics; 1:5 dilution). Following a fixation and permeabilization step (Foxp3 staining kit, eBiosciences), cells were stained with an anti-XPR1 antibody (4174-1-AP, Proteintech; 1:100 dilution) and secondary Brilliant Violet 421-labelled donkey anti-rabbit IgG (Biolegend; 1:1,000 dilution). A corresponding isotype control antibody (anti-rabbit IgG, I-1000, Vector Laboratories) was used for control. Megakaryocytes were identified as CD41^{high}CD42b^{high} population and were analyzed by flow cytometry analysis, as described previously [6, 7]. Washed murine platelets were stained with annexin V (Invitrogen, 1:20 dilution), anti-CD31 (clone: 390,

Miltenyi; 1:10 dilution) and anti-CD42b antibodies. Platelets were activated with thrombin (1 U ml^{-1}) and collagen-related peptide (CRP, 10 µg ml^{-1}). Analysis of murine XPR1 was performed as above. Moreover, in some experiments HEK293 cells were transiently transfected with mock pcDNA3.1 plasmid or constructs encoding XPR1 or XPR1-GFP fusion proteins prior to XPR1 detection by flow cytometry. XPR1 signal correlated with XPR1 transfection. Furthermore, in XPR1-GFP overexpressing but not in mock-transfected cells, GFP expression correlated with XPR1 detection validating the specificity of XPR1 antibody. Fc receptor-binding was prevented by using anti-CD16/CD32 blockade (clone: 2.4G2, BD Biosciences) and isotype control antibodies (BD Biosciences). Flow cytometry data were acquired on a BD FACSCanto machine (BD Biosciences) and data were analyzed using FlowJo v10.0.7 software (Treestar).

ATP measurements in platelets

ATP levels in platelets from *Xpr1*$^{fl/fl}$ and *Xpr1*$^{fl/fl}$ *Pf4-Cre* mice were measured using the Luminescent ATP Detection Kit (Abcam) according to the manufacturer´s instruction. Briefly, platelets were lysed and following addition of luciferase and luciferin, emitted light was measured using a VICTOR3 luminometer (PerkinElmer).

Plasmids and small interfering RNA (siRNA)

A hemagglutinin (HA)-tagged version of human *XPR1* cloned into the pCHIX expression vector was kindly provided by Dr. Jean-Luc Battini, Montpellier, France. The empty pCHIX vector was used as mock control. Sequences of siRNA (Integrated DNA Technologies) targeting the 3´UTR of human *XPR1* were as follows: 5´-GGAUUUCAUGCCAUCCCAUTT-3´and 5´-GCACUUCCACCAUGUAUUAUT-3´ [8]. siRNA directed to the firefly luciferase gene was used as control (Thermo Scientific).

Genotyping of mice

Genotyping was performed using a forward primer located in the Pf4-promoter (CCAAGTCCTACTGTTTCTCACTC) and a reverse primer in the Cre-cDNA (TGCACAGTCAGCAGGTT) yielding a 420 bp polymerase chain reaction (PCR) product. For genotyping of *Xpr1*-floxed mice, the following primers were used: ATGTAGGCCCAGTGTTTATCTTTAGGAT and ATGGGAAAATGAAGACACACCTGAA yielding a 322 bp and 261 bp product for the *Xpr1*-floxed and the wild-type allele, respectively.

Cell transfection

250 nM siRNA and indicated amounts of DNA vectors were transfected into HEK293 and

MEG-01 cells using Lipofectamine 2000 (Thermo Scientific) and Nucleofector technology (Nucleofector Solution C; Lonza), respectively. All transfections were done according to the manufacturers´ instructions.

Solubilization of platelet membranes

Human platelets were obtained from fresh apheresis platelet concentrate (leukocyte depleted; 1.1×10^9 platelets ml^{-1}; Karolinska Universitetssjukhuset, Stockholm, Sweden). Platelet concentrates were centrifuged at 100 *g* for 10 min to remove potential contaminating leukocytes or erythrocytes. To remove residual plasma proteins, the resultant pellets were washed twice with phosphate buffer saline (PBS). Final pellets were stored at -80°C until further use. Platelet membranes were solubilized using NP-40 detergent. Briefly, platelets were lysed in the presence of hypotonic buffer (5 mM Tris-HCl, 2 mM EDTA; pH 7.6). After centrifugation at 400 *g* for 10 min at 4°C, the supernatant was collected and centrifuged at 30,000 *g* for 20 min at 4°C. The pellet was resuspended with solubilization buffer (150 mM NaCl, 1% NP-40, 50 mM Tris; pH 7.4; protease inhibitor tablet [Roche]) for 60 min under agitation at 4°C. Afterwards, the suspension was centrifuged for 30 min at 20,000 *g* at 4°C.

Immunoblotting

Platelet membrane fractions or cultured cell lysates were resuspended in 1x SDS sample buffer (50 mM Tris-HCl, 2% SDS, 10% glycerol, 100 mM β-mercaptoethanol; pH 6.8), subjected to lysis in a sonicator and resolved by 10% SDS PAGE under reducing conditions. The separated proteins were blotted onto Hybond-C Extra nitrocellulose membranes (GE Healthcare). Proteins from membrane fractions were probed using antibodies directed against the XPR1 N-terminus (HPA016563, 4 µg ml^{-1}; Sigma-Aldrich) or XPR1 C-terminus (HPA016557; Sigma-Aldrich; 3 µg ml^{-1}). Proteins from cell lysates were immunoblotted using α-XPR1 (HPA016557; 0.8 µg ml^{-1}) or α-VASP (M4; 1:250) antibodies [9]. Bound antibodies were detected by peroxidase-conjugated secondary antibody (donkey anti-rabbit, 1:5,000; Jackson ImmunoResearch Laboratories) followed by chemiluminescence detection method. HEK293 cells transiently transfected with pCHIX-XPR1 plasmid were used as positive controls. Signal intensities of blots were quantified using ImageJ software.

Real-Time PCR

mRNA *XPR1* expression of HEK-293 or MEG-01 cells was determined on day 1 to 5 after transfection using Cell-To-Ct kit (Thermo Scientific) and according to manufacturer's instructions. Briefly, 24 h after transfection, cells were detached and seeded in a 96-well plate. At indicated time points, cells were washed with PBS, mixed with Lysis Solution and incubated

for 5 min. Stop Solution was mixed into the lysate to inactivate the lysis reagents and the resultant lysates were used in a one-step real-time PCR with a TaqMan Gene Expression assay for *XPR1* gene (Hs00173707_m1; Thermo Scientific); 18S rRNA (Hs99999901_s1; Thermo Scientific) was used as the housekeeping gene. mRNA was isolated from mouse platelets and megakaryocytes (RNeasy kit, Qiagen) and transcribed into cDNA (SuperScript IV Vilo, Thermo Fisher). Real-time PCR was performed on StepOnePlus Real-time PCR instrument (Applied Biosystems). *Xpr1*-specific expression was analyzed using the Taqman probe Mm00495501_m1 (exon 14/15 junction region). *Platelet factor 4* (*Pf4*)- and *hypoxanthine phosphoribosyltransferase 1* (*Hprt1*)-specific Taqman probes Mm00451315_g1 and Mm00446968_m1 were used for housekeeping genes in platelets and megakaryocytes, respectively. Relative gene expression was calculated using the *2−ΔΔCt* method; values obtained from *Xpr1*^{fl/fl} mice were set to 100%.

PolyP electrophoresis

PolyP was separated by electrophoresis on 12% polyacrylamide tris-borate-EDTA buffer (TBE)-urea (7 M) gels and visualized by negative DAPI staining, as previously described [10]. Gels were agitated for 30 min in 2.5 µg ml^{-1} DAPI in fixative solution (20% methanol, 5% glycerol, pH 10.4) and then de-stained for 1 h in fixative solution without DAPI. Images were acquired using the Chemi Genius2 Bio Imaging System and the Syngene software (Syngene). In some experiments, polyP extracts pre-incubated with PPX (10 µg ml^{-1}) for 1 hour at 37°C prior to separation, were used as control.

Immunofluorescence microscopy

Resting platelets were plated onto glass coverslips, fixed with 2% paraformaldehyde and blocked with 1% bovine serum albumin (BSA). Platelets were then incubated with α-XPR1 primary antibody (HPA016563, Merck, 4 µg ml^{-1}) for 1 h at RT, followed by the fluorescein isothiocyanate-conjugated secondary antibody (1:80, Sigma) or α-GPIb-phycoerythrin (PE, R&D Systems) antibody for 1 hour. Platelets were permeabilized with saponin and GPIb was stained with anti-CD42 antibody (Emfret Analytics). PolyP was visualized using 6xHis-tagged PPX_Δ12 probe [10] and fibrin was stained as described before [11]. Slides were assessed using a Leica confocal microscope and images were acquired using the LAS X software (Leica).

Cloning of Murine Leukemia Virus (MLV) envelope-derived ligands

The following primers were used to clone expression constructs for the N-terminal 259 or 262 amino-acids of the Receptor-Binding Domains (RBD) of X-MLV or P-MLV, respectively: 5′-CAC*CTCGAG*AGGTTCAGCGTTCTCAAAACCCCTT-3′ and 5′-

CTG*AAGCTT*CTTACCTGGGGAGCATGATCTGCACGGG-3' for X-MLV; and 5´-CAC*CTCGAG*AGGTCCAGCGTTCTCAAAA-3´ and 5´-CTG*AAGCTT*CTTATATATTGAGGACCTGG-3' for P-MLV (restriction sites are indicated in italics). XhoI and HindIII restriction sites were used to insert the amplified DNA fragment into the pTrcHisB expression vector (Invitrogen) leading to pTrcHisB-XVDL or pTrcHisB-PVDL.

Expression and purification of XVDL and PVDL

Ultracompetent *E. coli* cells were transformed with pTrcHisB vectors coding XVDL or PVDL. Recombinant protein expression was induced by 0.5 mM isopropylthio-β-d-galactoside (Sigma-Aldrich) at 37 °C for 4 h. Bacteria were collected by centrifugation, resuspended in binding buffer (20 mM NaH_2PO_4, 500 mM NaCl and 20 mM imidazole; pH 7.4) and lysed by sonication. Cell lysates were centrifuged (10,000 *g* for 10 min at 4°C) and supernatants were loaded on 1 ml HisTrap FF crude column (GE Healthcare). Following washing, bound proteins were eluted with 20 mM NaH_2PO_4, 500 mM NaCl and 500 mM imidazole, pH 7.4. Fractions containing proteins were combined and solvent was changed to PBS pH 7.4, using desalting columns (Econo-Pac 10 DG, Bio-Rad). Protein concentration was determined by the Bradford assay. Coomassie brilliant blue staining assessed protein purity. Western blotting was performed using 6xHis-tag antibody (1:1,000, Merck Millipore) and horseradish peroxidase (HRP)-coupled anti-mouse Fc antibody (1:5,000, Jackson ImmunoResearch).

Real-time thrombin generation

Thrombin formation in real time was determined with the calibrated automated thrombography (CAT) method using a Fluoroscan Ascent fluorometer (Thermo Scientific) equipped with a dispenser (Thrombinoscope BV) [11]. In brief, coagulation in XVDL and PVDL (2-200 µg ml^{-1})-supplemented PRP was stimulated by Horm collagen (33.3 µg ml^{-1}, Takeda) in 120 µl containing 16.6 mM Ca^{2+} and 2.5 mM fluorogenic substrate (ZGGR-AMC, Thrombinoscope BV). Alternatively, thrombin formation was initiated by addition of 4 U ml^{-1} activated factor X (FXa, Haemtech) to PRP of *Xpr1$^{fl/fl}$ Pf4-Cre* and *Xpr1$^{fl/fl}$* mice. In some experiments, FXIIa inhibitory antibody 3F7 (100 µg ml^{-1}), Infestin-4 fused to recombinant human albumin (rHA-Infestin-4, 500 µg ml^{-1}), PPX (500 µg ml^{-1}), or PPX_Δ12 (500 µg ml^{-1}) were added to plasma samples and preincubated for 30 min prior to stimulation. Thrombin formation was quantified using the Thrombinoscope software package (Version 3.0.0.29). In some experiments thrombin formation was measured by conversion of the chromogenic substrate S2238 (1 mM, Chromogenix).

Thrombus formation under flow

Thrombus formation under flow was analyzed as described previously [11] with some minor modifications. Coverslips were coated with Horm collagen (0.5 μg applied to 10 mm^2) and blocked with HEPES buffer (136 mM NaCl, 2.7 mM KCl, 0.42 mM NaH$_2$PO$_4$, 5 mM HEPES, 2 mM MgCl$_2$ and 1% BSA, pH 7.4) for 30 min. Coverslips were placed onto a transparent, 50 μm deep parallel-plate flow chamber (Maastricht Instruments BV) which was pre-rinsed with BSA-containing buffer. Chambers were co-infused with citrate anticoagulated blood and isotonic CaCl$_2$/MgCl$_2$ solution (10:1 ratio) by pulse-free pumps, which resulted in free Ca^{2+} and Mg^{2+} concentrations of ~2 mM each. Citrated blood samples were pre-incubated for 4 h with rising concentrations of purified XVDL (0–200 μg ml^{-1}). After 4 min of flow (shear rate of 100 s^{-1} for venous or 1,000 s^{-1} for arterial flow conditions), flow chambers were rinsed with HEPES buffer (pH 7.4) containing 2 mM CaCl$_2$. Phase-contrast images were recorded on an ORCA-Flash 2.8 CMOS Camera (Hamamatsu) and Nikon Eclipse Ti microscope equipped with a 20x objective. The surface area covered with thrombus was determined in each image using ImageJ software.

Blood collection

Peripheral venous blood from healthy volunteers was collected into 3.2% trisodium citrate (9:1, blood-to-citrate ratio). All participants provided written informed consent. The protocol, amendments, and informed consent forms were approved by the institutional review board and human subject accrual was conducted in accordance with the principles of the Declaration of Helsinki. Platelet-rich plasma (PRP) was prepared by centrifugation at 250 g for 10 min.

For murine plasma isolation, mice were anesthetized by intraperitoneal injection of 2,2,2-tribromoethanol and 2-methyl-2-butanol and subjected to retro-orbital blood sampling. Blood was collected into 3.2% trisodium citrate and PRP was obtained by differential centrifugation of citrated blood at 100 g for 10 min followed by 60 g for 8 min.

Platelet aggregometry

Heparinized whole blood taken from the retro-orbital plexus was centrifuged at 160 g for 15 to obtain mouse PRP. Following addition of 40 ng ml^{-1} prostaglandin E1 (Sigma) and 10 μM indomethacin (Sigma) platelets were collected (600 g, 10 min), resuspended in HEPES-Tyrode's buffer and normalized to 150 x 10^6 platelets ml^{-1} using a ProCyte Dx instrument (IDEXX laboratories). Samples with lower platelet counts were excluded from the analyses. Aggregation was induced by addition of 10 or 5 μg ml^{-1} Horm collagen or 1.5 μg ml^{-1} ristocetin and monitored for 10 min using a light transmission aggregometer 490 4+4 (Chrono-Log).

Tail bleeding assays

Bleeding times were determined as previously described [3]. Mice were anesthetized and the mouse tail was transected 3 mm from the tip with a razor blade. The bleeding tail was immersed in a 15 ml test tube containing 12 ml pre-warmed PBS. Bleeding time was recorded as the time to cessation of bleeding for 10 s. Blood loss was quantified by measuring the hemoglobin content of blood collected into PBS. Following centrifugation, the pellet was lysed with lysis buffer (8.3 g l^{-1} NH_4Cl, 1.0 g l^{-1} $KHCO_3$ and 0.037 g l^{-1} EDTA) and absorbance of the sample was measured at 575 nm. ROUT analysis of tail bleeding time identified six data points that were excluded for subsequent analysis. Additionally, tail-bleeding times were analyzed with a filter paper dabbed to the wound at 5 sec intervals without disrupting the forming clot. The experiment was continued until cessation of bleeding.

Statistical analysis

All data are presented as mean ± standard error of the mean (SEM) unless otherwise indicated. Difference between two groups was determined by unpaired 2-tailed Student's t-test. One-way ANOVA analysis with Tukey multiple comparisons test was used to compare 3 or more related groups. All *P* values are two-tailed; *P* values less than 0.05 were considered statistically significant. Data were analyzed using GraphPad Prism 8.0 (GraphPad Software). Sample size calculation for each assay was based on previous studies [2,12,13] using the British Columbia University online statistical platform (https://www.stat.ubc.ca/~rollin/stats/ssize/n2.html). Assuming a power of 80% and an alpha error of 0.05, we calculated that 6 animals (for carotid occlusion), 5 animals (for pulmonary thrombosis) and 7 animals (for bleeding assays) would be required in each group for a two-sided test of the null hypothesis, respectively. Outliers were identified by ROUT test (GraphPad Prism).

Data availability

The authors declare that data presented in this manuscript and experimental tools are available upon request to Dr. Thomas Renné, thomas@renne.net.
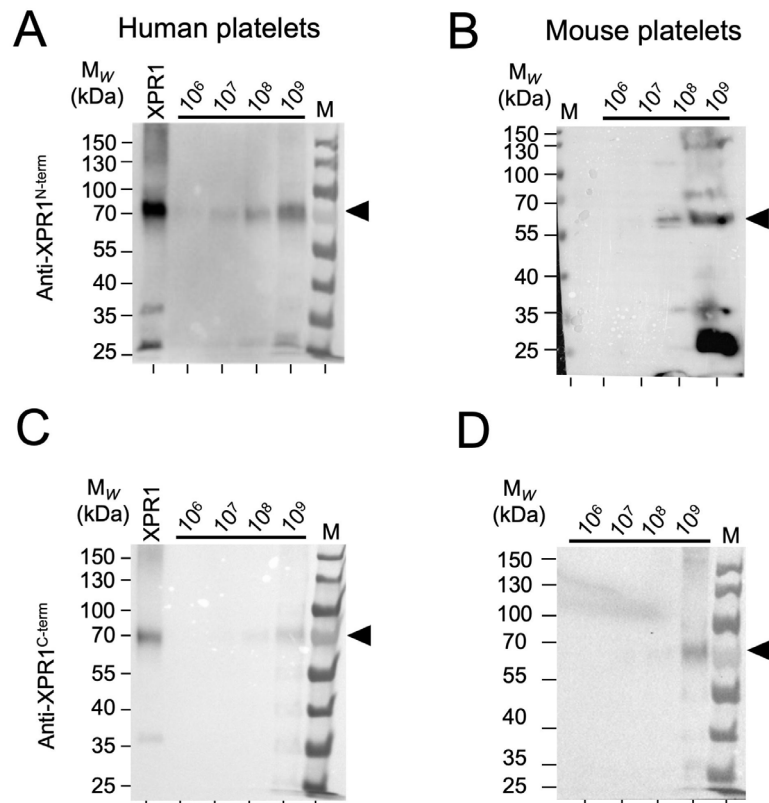
SUPPLEMENTAL FIGURE 1. Full length western blots of cropped images shown in Figure 1B and 1C.

Images represent merged scans of colorimetric size standard bands and XPR1 chemiluminescent western blot analyses. Arrows indicate XPR1 detected by antibodies against the (**A**, **B**) N- and (**C**, **D**) C-terminus of the protein, respectively. Numbers of loaded (**A**, **C**) human and (**B**, **D**) mouse platelets are indicated on the top.
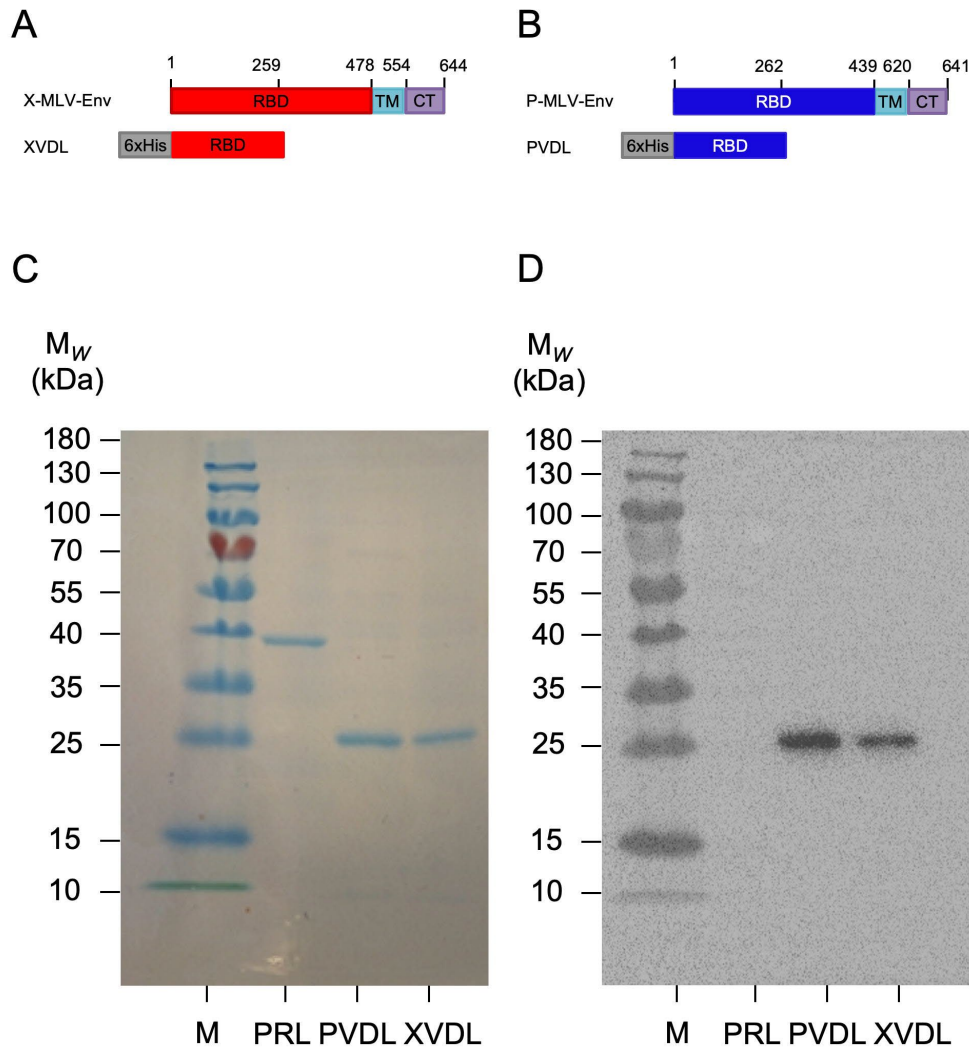
SUPPLEMENTAL FIGURE 2. Cloning and recombinant expression of a XPR1-blocking ligand.

(**A-B**) Schematic representation of xenotropic (X-MLV-Env) and polytropic murine leukemia virus envelope (P-MLV-Env) and xenotropic (XVDL) and polytropic (PVDL) virus-derived ligands. The receptor binding domain (RBD), the transmembrane subunit (TM) and the cytoplasmatic tail (TC) are indicated. Both constructs were fused to an N-terminal 6xHis-tag. *E. coli* expressed and affinity chromatography-purified recombinant XVDL and PVDL were separated by SDS-PAGE and visualized by (**C**) Coomassie brilliant blue staining or (**D**) western blotting with an antibody against the 6xHis-tag. Bacterial expressed proline-rich domain of factor XII (PRL) was loaded as control. A representative full-size gel and immunoblot are shown in panels (**C**) and (**D**), respectively, *n*=3.
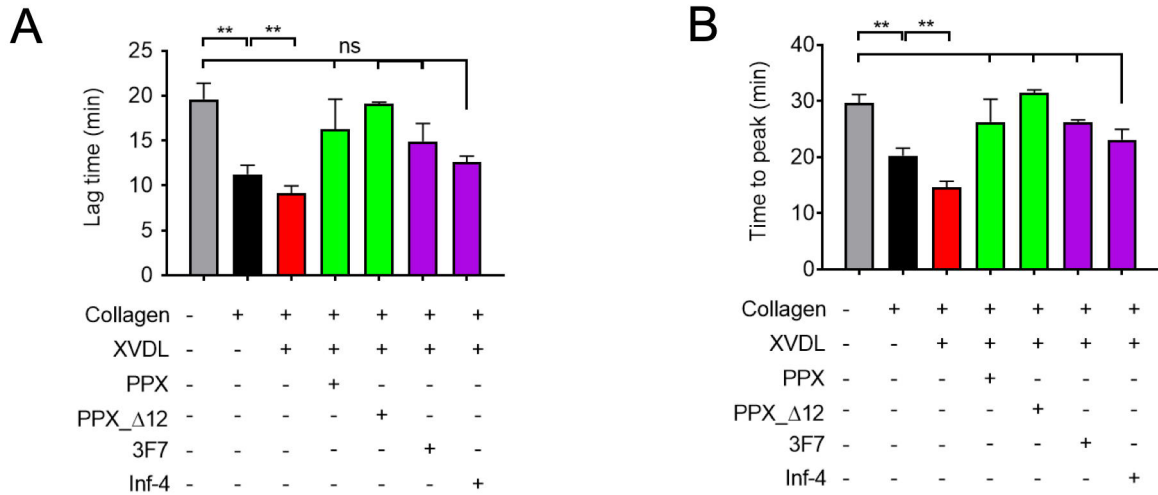
SUPPLEMENTAL FIGURE 3. Pharmacologic targeting of XPR1 increases activated platelet-driven thrombin formation via the polyP/FXII pathway.

Lag time (**A**) and time to peak thrombin (**B**) formation in collagen-stimulated human PRP treated with XVDL (200 µg ml⁻¹, 4 h), in the presence of PPX (500 µg ml⁻¹), PPXΔ12 (500 µg ml⁻¹), 3F7 (650 nM) or infestin-4 (500 µg ml⁻¹). Data correspond to Figures 3H - 3K and are expressed as mean values ± SEM; *n*=3. One-way ANOVA and Tukey's multiple comparison test was performed for statistical analysis ** *P*<0.01, n.s. non-significant.
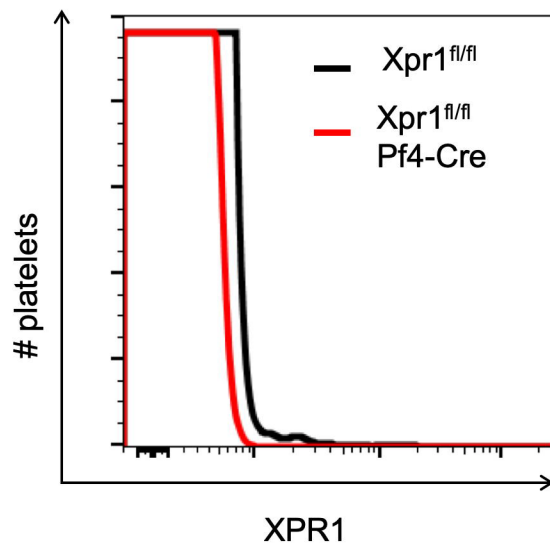
SUPPLEMENTAL FIGURE 4. XPR1 expression on murine platelets.

Flow cytometry analysis of XPR1 expression on freshly isolated washed platelets gated on CD31+CD42b+ populations from *Xpr1$^{fl/fl}$* and *Pf4-Cre Xpr1$^{fl/fl}$* mice.
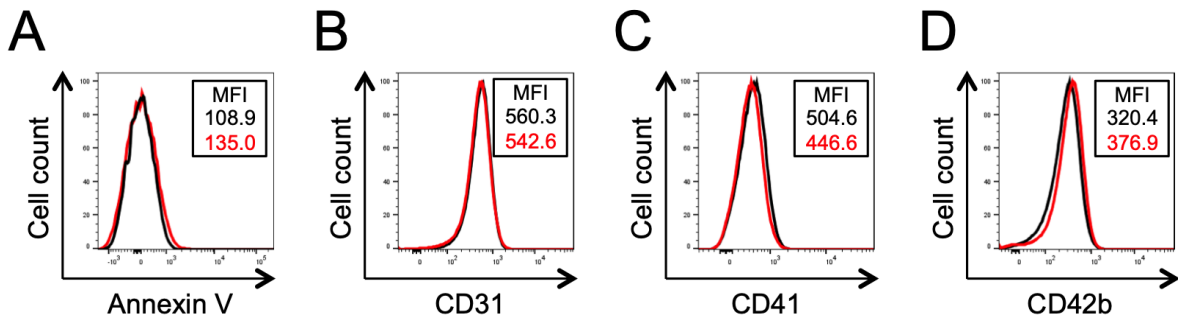
SUPPLEMENTAL FIGURE 5: Phosphatidylserine exposure and expression of surface markers on *Xpr1^fl/fl* and *Xpr1^fl/fl Pf4-Cre* platelets.

Flow cytometry analysis of phosphatidylserine exposure and key surface marker expression on washed platelets from *Xpr1^fl/fl* (black lines) and *Xpr1^fl/fl Pf4-Cre* (red lines) mice. (**A**) Platelets were activated with collagen-related peptide and thrombin and stained with FITC-annexin V. (**B-D**) Resting platelets were stained with antibodies against CD31 (B), CD41 (C) or CD42b (D). Mean fluorescence intensities (MFI) for the two genotypes are given in the upper right.
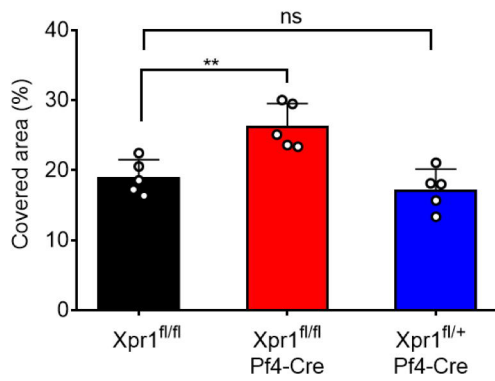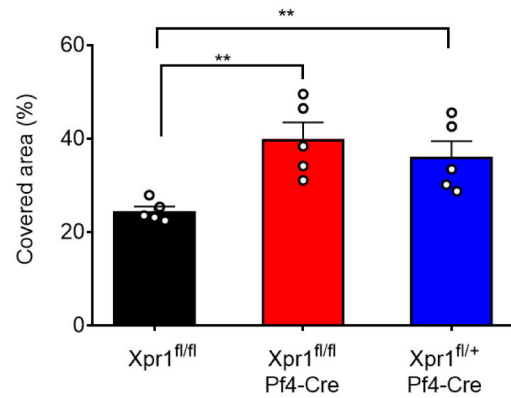
SUPPLEMENTAL FIGURE 6. Increased thrombus formation in blood from *Xpr1^fl/fl* Pf4-Cre mice under flow.

Recalcified citrated murine whole blood from *Xpr1^fl/fl*, *Xpr1^fl/fl Pf4-Cre* and *Xpr1^fl/+ Pf4-Cre* mice was perfused for 2 min over a collagen-coated surface at an arterial (1000 s^{-1}, **A**) or venous (100 s^{-1}, **B**) shear rate. Bar graphs depict the percentage of surface area covered by thrombi, expressed as mean values ± SD. One-way ANOVA and Tukey's multiple comparison test was performed for statistical analysis; *n*=5; **p<0.01, n.s. non-significant.
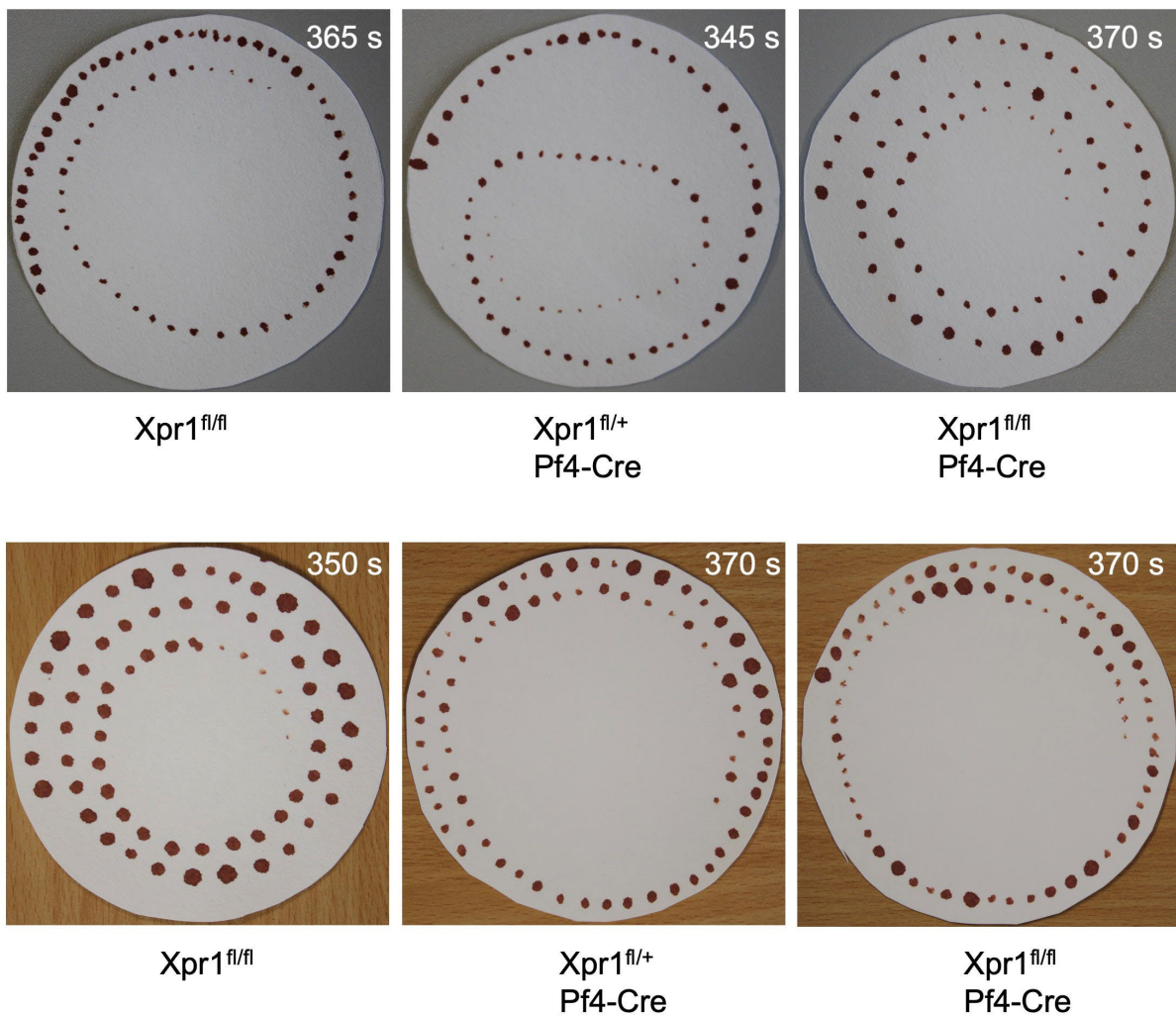
SUPPLEMENTAL FIGURE 7. Tail bleeding times in XPR1-deficient mice.

Blood drops were collected from *Xpr1*^{fl/fl} (left), *Xpr1*^{fl/+} *Pf4-Cre* (middle) and *Xpr1*^{fl/fl} *Pf4-Cre* (right) mice on a filter paper in 5 s intervals. Two representative filter papers are shown for each murine genotype. Time to cessation of bleeding is indicated in the upper right corner of each panel. Quantitation of data is provided in Figure 6G.

SUPPLEMENTAL REFERENCES

1   Labberton, L. *et al.* Neutralizing blood-borne polyphosphate in vivo provides safe thromboprotection. *Nature communications* **7**, 12616, doi:10.1038/ncomms12616 (2016).

2   Nickel, K. F. *et al.* The polyphosphate-factor XII pathway drives coagulation in prostate cancer-associated thrombosis. *Blood* **126**, 1379-1389, doi:10.1182/blood-2015-01-622811 (2015).

3   Renne, T. *et al.* Defective thrombus formation in mice lacking coagulation factor XII. *J Exp Med* **202**, 271-281, doi:10.1084/jem.20050664 (2005).

4   Slot, J. W. & Geuze, H. J. Cryosectioning and immunolabeling. *Nat Protoc* **2**, 2480-2491, doi:10.1038/nprot.2007.365 (2007).

5   Bender, M. *et al.* Dynamin 2-dependent endocytosis is required for normal megakaryocyte development in mice. *Blood* **125**, 1014-1024, doi:10.1182/blood-2014-07-587857 (2015).

6   Meinders, M. *et al.* Sp1/Sp3 transcription factors regulate hallmarks of megakaryocyte maturation and platelet formation and function. *Blood* **125**, 1957-1967, doi:10.1182/blood-2014-08-593343 (2015).

7   Chen, Z., Hu, M. & Shivdasani, R. A. Expression analysis of primary mouse megakaryocyte differentiation and its application in identifying stage-specific molecular markers and a novel transcriptional target of NF-E2. *Blood* **109**, 1451-1459, doi:10.1182/blood-2006-08-038901 (2007).

8   Legati, A. *et al.* Mutations in XPR1 cause primary familial brain calcification associated with altered phosphate export. *Nature genetics* **47**, 579-581, doi:10.1038/ng.3289 (2015).

9   Benz, P. M. *et al.* Cytoskeleton assembly at endothelial cell-cell contacts is regulated by alphaII-spectrin-VASP complexes. *J Cell Biol* **180**, 205-219, doi:10.1083/jcb.200709181 (2008).

10   Verhoef, J. J. *et al.* Polyphosphate nanoparticles on the platelet surface trigger contact system activation. *Blood* **129**, 1707-1717, doi:10.1182/blood-2016-08-734988 (2017).

11   Larsson, M. *et al.* A factor XIIa inhibitory antibody provides thromboprotection in extracorporeal circulation without increasing bleeding risk. *Sci Transl Med* **6**, 222ra217, doi:10.1126/scitranslmed.3006804 (2014).

12   de Maat, S. *et al.* Design and characterization of alpha1-antitrypsin variants for treatment of contact system-driven thromboinflammation. *Blood* **134**, 1658-1669, doi:10.1182/blood.2019000481 (2019).

13   Muller, F. *et al.* Platelet polyphosphates are proinflammatory and procoagulant mediators in vivo. *Cell* **139**, 1143-1156, doi:10.1016/j.cell.2009.11.001 (2009).
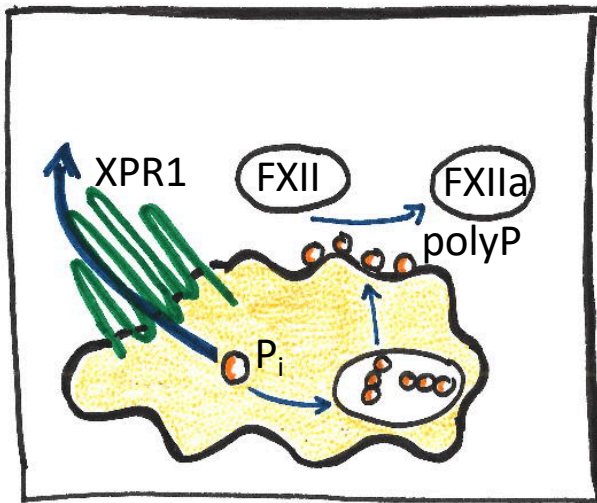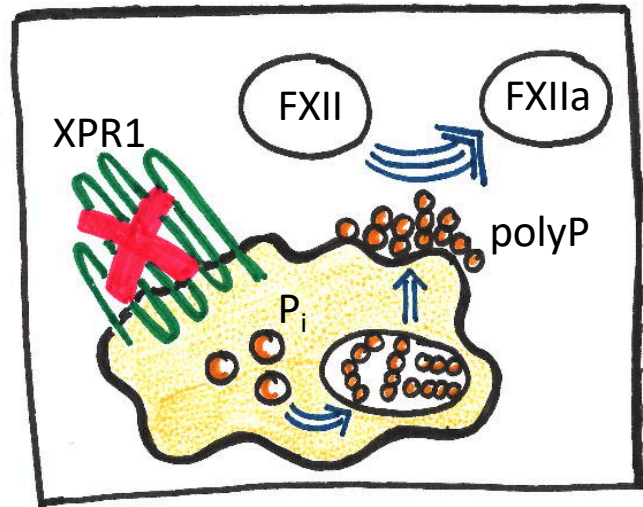
Platelet XPR1 regulates procoagulant polyphosphate. The phosphate (P_i) exporter Xenotropic and Polytropic retrovirus Receptor 1 (XPR1) regulates P_i with implications for polyphosphate (polyP) content in platelets. Activated platelets release polyP from their dense granules that is retained on the plasma membrane and activates factor XII (FXII) leading to thrombosis. Genetic or pharmacologic targeting of XPR1 facilitates accumulation of polyP resulting in increased risk of thrombosis.

Visual Abstract